Molecular Therapy
Original Article

miR-486 attenuates cardiac ischemia/reperfusion injury and mediates the beneficial effect of exercise for myocardial protection

Yihua Bei,[1,2,9] Dongchao Lu,[3,4,9] Christian Bär,[3,4,9] Shambhabi Chatterjee,[3] Alessia Costa,[3,4] Isabelle Riedel,[3] Frank C. Mooren,[5] Yujiao Zhu,[1,2] Zhenzhen Huang,[1,2] Meng Wei,[1,2] Meiyu Hu,[1,2] Sunyi Liu,[6] Pujiao Yu,[6] Kun Wang,[7] Thomas Thum,[3,4,8] and Junjie Xiao[1,2]

[1]Cardiac Regeneration and Ageing Lab, Institute of Geriatrics (Shanghai University), Affiliated Nantong Hospital of Shanghai University (The Sixth People's Hospital of Nantong), School of Medicine, Shanghai University, Nantong 226011, China; [2]Shanghai Engineering Research Center of Organ Repair, School of Life Science, Shanghai University, Shanghai 200444, China; [3]Institute of Molecular and Translational Therapeutic Strategies, Hannover Medical School, 30625 Hannover, Germany; [4]REBIRTH Center for Translational Regenerative Medicine, Hannover Medical School, 30625 Hannover, Germany; [5]Witten/Herdecke University, Faculty of Health/School of Medicine, 58448 Witten, Germany; [6]Department of Cardiology, Tongji Hospital, Tongji University School of Medicine, Shanghai 200065, China; [7]Department of Cardio-thoracic Surgery, The Second Affiliated Hospital of Xuzhou Medical University, Xuzhou 221002, China; [8]Fraunhofer Institute for Toxicology and Experimental Medicine, 30625 Hannover, Germany

Exercise and its regulated molecules have myocardial protective effects against cardiac ischemia/reperfusion (I/R) injury. The muscle-enriched miR-486 was previously identified to be upregulated in the exercised heart, which prompted us to investigate the functional roles of miR-486 in cardiac I/R injury and to further explore its potential in contributing to exercise-induced protection against I/R injury. Our data showed that miR-486 was significantly downregulated in the heart upon cardiac I/R injury. Both preventive and therapeutic interventions of adeno-associated virus 9 (AAV9)-mediated miR-486 overexpression could reduce cardiac I/R injury. Using AAV9 expressing miR-486 with a cTnT promoter, we further demonstrated that cardiac muscle cell-targeted miR-486 overexpression was also sufficient to protect against cardiac I/R injury. Consistently, miR-486 was downregulated in oxygen-glucose deprivation/reperfusion (OGDR)-stressed cardiomyocytes, while upregulating miR-486 inhibited cardiomyocyte apoptosis through PTEN and FoxO1 inhibition and AKT/mTOR activation. Finally, we observed that miR-486 was necessary for exercise-induced protection against cardiac I/R injury. In conclusion, miR-486 is protective against cardiac I/R injury and myocardial apoptosis through targeting of PTEN and FoxO1 and activation of the AKT/mTOR pathway, and mediates the beneficial effect of exercise for myocardial protection. Increasing miR-486 might be a promising therapeutic strategy for myocardial protection.

INTRODUCTION

Timely and effective cardiac reperfusion is the key strategy to limit infarct size after acute myocardial infarction (AMI).[1] The mortality from AMI has decreased during past decades where interventional reperfusion is available; however, reperfusion per se will inevitably cause further injury to the myocardium, which may develop cardiac remodeling and eventually heart failure (HF).[2,3] Effective strategies to reduce cardiac ischemia/reperfusion (I/R) injury are still lacking.[4]

MicroRNAs (miRNAs, miRs) are a large class of small non-coding RNAs regulating target genes at the post-transcriptional level, and they play important roles in cardiovascular physiology and disease.[5] miRNA-486-5p (miR-486) is a skeletal and cardiac muscle-enriched miRNA encoded by the muscle-specific gene *Ankyrin*, which was found to be decreased in atrophied skeletal muscle but increased during postnatal cardiac growth.[6] Increasing evidence indicates that cardiac-enriched miRNAs, such as miR-1, miR-133a, miR-208a/b, and miR-499, are critically involved in cardiogenesis and cardiac function.[7] In the cardiovascular system, miR-486 was previously shown to prevent hydrogen peroxide (H_2O_2)-induced and coronary microembolization-induced cardiomyocyte apoptosis,[8,9] and to mediate the protective effect of circulating extracellular vesicles against cardiomyocyte apoptosis.[10] However, the functional roles and regulatory mechanisms of miR-486 in cardiac I/R injury remain to be elucidated.

Received 6 June 2021; accepted 20 January 2022;
https://doi.org/10.1016/j.ymthe.2022.01.031.

[9]These authors contributed equally

Correspondence: Junjie Xiao, PhD, Cardiac Regeneration and Ageing Lab, Institute of Geriatrics (Shanghai University), Affiliated Nantong Hospital of Shanghai University (The Sixth People's Hospital of Nantong), School of Medicine, Shanghai University, Nantong 226011, China; Shanghai Engineering Research Center of Organ Repair, School of Life Science, Shanghai University, Shanghai 200444, China.
E-mail: junjiexiao@shu.edu.cn
Correspondence: Thomas Thum, PhD, Institute of Molecular and Translational Therapeutic Strategies, Hannover Medical School, Hannover 30625, Germany.
E-mail: thum.thomas@mh-hannover.de

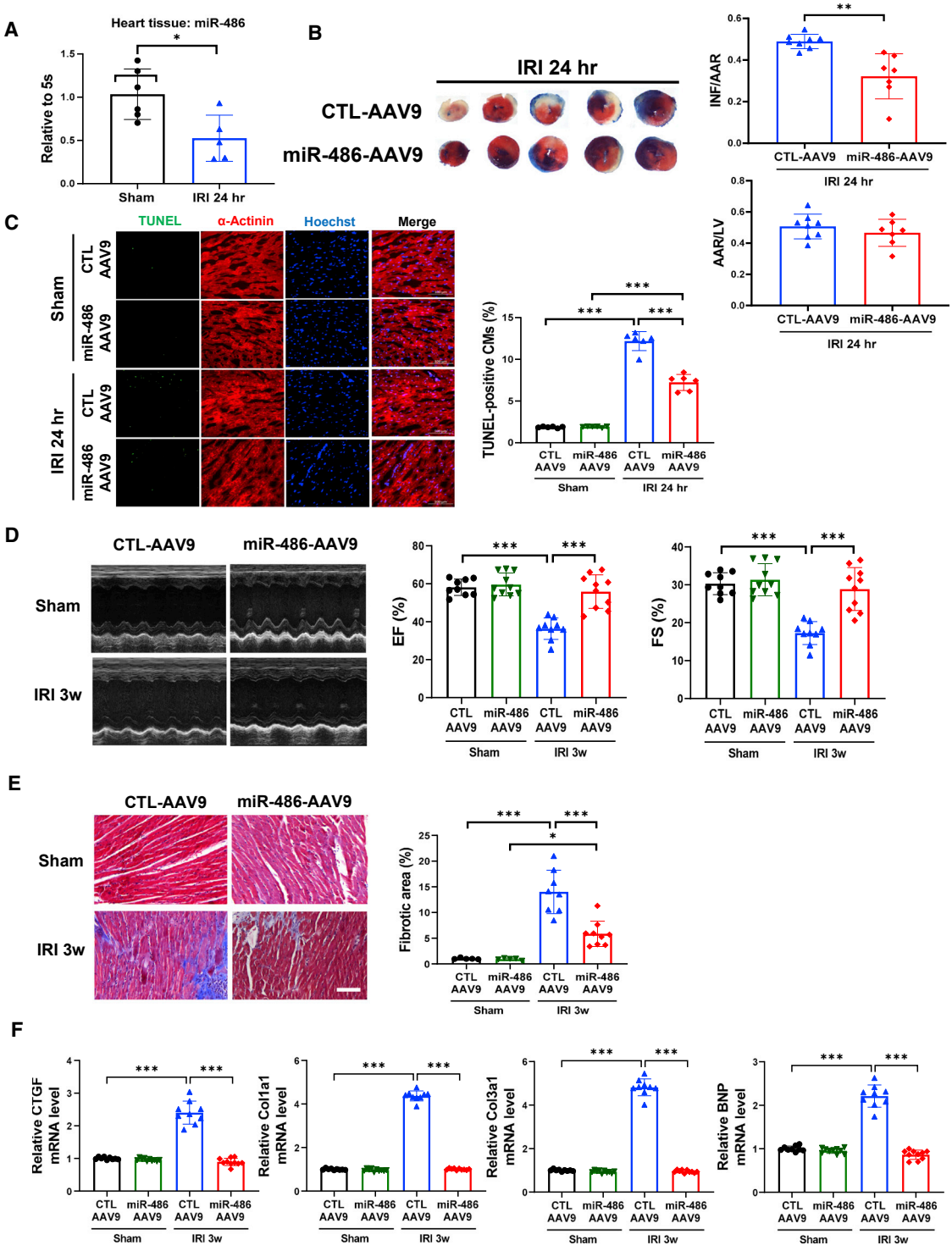

Figure 1. AAV9-mediated miR-486 overexpression prevents cardiac ischemia/reperfusion injury

(A) RT-PCR for miR-486 expression in heart tissues from mice at 24 h after cardiac ischemia/reperfusion (I/R) injury compared with sham controls (n = 5–6). (B) The 2,3,5-triphenyltetrazolium chloride (TTC) staining for the infarct size at 24 h after cardiac I/R injury as determined by the infarct-size/area-at-risk (INF/AAR) ratio. The area-at-risk/left-ventricle-weight (AAR/LV) ratio represents the homogeneity of surgery (n = 7–8). (C) TUNEL staining for myocardial apoptosis in α-actinin-labeled cardiomyocytes (n = 6). Scale bar, 100 μm. (D) Echocardiography for left-ventricular ejection fraction (EF, %) and fractional shortening (FS, %) in mice at 3 weeks after I/R injury (n = 9–10). (E) Masson

(legend continued on next page)

Exercise is an effective and economical way to prevent and treat cardiovascular diseases.[11,12] In experimental cardiac I/R injury models, chronic exercise training was proved to be effective at reducing infarct size.[13] Interestingly, exercise-regulated molecules also have the potential to exert myocardial protective effects.[14–17] miR-486 was previously found to be upregulated in the heart after exercise training.[18] However, the relationship between exercise and miR-486, and whether miR-486 could contribute to exercise-induced protection against cardiac I/R injury, was largely unclear.

In the present study, we investigated the functional roles of miR-486 in murine models of cardiac I/R injury and an oxygen-glucose deprivation/reperfusion (OGDR)-induced apoptosis model of cardiomyocytes. We further identified target genes and molecular mechanisms underlying the myocardial protective effect of miR-486. Also, we explored the potential regulatory effect of exercise on miR-486 and the role of miR-486 in exercise-induced protection against cardiac I/R injury.

RESULTS

miR-486 overexpression prevents cardiac I/R injury and cardiac dysfunction

To study the functional roles of miR-486 in regulating cardiac I/R injury, we first examined the change in miR-486 expression after cardiac I/R injury. A marked downregulation of miR-486 was observed in heart tissues from a murine model of cardiac I/R injury *in vivo* (Figure 1A). To further investigate the functional roles of miR-486 *in vivo*, mice injected with adeno-associated virus 9 (AAV9) expressing miR-486 (miR-486-AAV9) were subjected to acute cardiac I/R injury (Figure S1A). miR-486 was significantly upregulated in mouse heart tissues after miR-486-AAV9 injections (Figure S1B). At 24 h after cardiac I/R injury, mice with AAV9-mediated miR-486 overexpression in the heart had significantly reduced infarct size compared with those injected with AAV9 controls (CTL-AAV9) (Figure 1B). Moreover, miR-486 significantly reduced TUNEL-positive cardiomyocytes (Figure 1C), decreased Bax/Bcl-2 ratio and caspase-3 cleavage (Figure S1C), and downregulated CTGF, Col1a1, Col3a1, and BNP mRNA levels (Figure S1D) in mouse hearts upon acute I/R injury. These data demonstrate markedly protective effects of miR-486 against acute cardiac I/R injury *in vivo*.

To further investigate whether miR-486 overexpression could protect the heart in the long term, we injected mice with miR-486-AAV9 and then subjected them to cardiac I/R injury for 3 weeks (Figures S2A and S2B). At 3 weeks post I/R injury, mice injected with miR-486-AAV9 had well-preserved cardiac function compared with the CTL-AAV9-injected I/R group (Figure 1D). Meanwhile, miR-486 overexpression reduced the Bax/Bcl-2 ratio and caspase-3 cleavage (Figure S2C), and also reduced cardiac fibrotic areas (Figure 1E) and downregulated CTGF, Col1a1, Col3a1, and BNP expression (Figure 1F) in mouse hearts after cardiac I/R injury. During a 6-week long-term functional experiment of miR-486 *in vivo*, we observed that only three mice died post I/R injury in the CTL-AAV9 + I/R injury (IRI) group, while no mice died in the sham groups or in the I/R group injected with miR-486-AAV9, indicating a low mortality due to the I/R surgery in our study. Although no difference was found in the survival rate among different groups (Figure S3A), the beneficial effect of miR-486 was still obvious in attenuated cardiac remodeling and cardiac dysfunction at 6 weeks after I/R injury (Figures S3B–S3E).

In contrast, we constructed an miR-486 sponge AAV9 to examine the functional role of inhibiting miR-486 in cardiac I/R injury. We first observed that inhibiting miR-486 did not further increase the infarct size at 24 h after I/R injury (Figure S4A). Next, miR-486 sponge AAV9 was injected via tail vein at 1 week before cardiac I/R injury, and heart tissues were harvested at 3 weeks post I/R injury (Figure S4B). We demonstrated that miR-486 sponge AAV9 significantly reduced miR-486 expression levels in heart tissues (Figure S4C). Meanwhile, luciferase reporter assay verified that miR-486 sponge was able to target and bind miR-486 directly, but had no binding activity with other miRNAs such as miR-210 (Figure S4D). However, inhibiting miR-486 was not able to further aggravate cardiac I/R injury and cardiac dysfunction at 3 weeks post I/R injury (Figures S4E–S4H).

Taken together, these data indicate that miR-486 overexpression is sufficient to prevent myocardial apoptosis, cardiac remodeling, and cardiac dysfunction after I/R injury

Therapeutic delivery of miR-486-AAV9 attenuates cardiac I/R injury and cardiac dysfunction

To investigate further whether delivery of miR-486-AAV9 shortly after myocardial reperfusion still had a beneficial effect, we treated mice with miR-486-AAV9 through tail vein injection within 30 min of cardiac I/R injury (Figure 2A). At 3 weeks post I/R injury, an increase in miR-486 expression was confirmed in heart tissues from mice treated with miR-486-AAV9 (Figure 2B). Moreover, therapeutic delivery of miR-486-AAV9 had beneficial effects in attenuating cardiac dysfunction, cardiac fibrosis, and apoptosis in mice with cardiac I/R injury (Figures 2C–2F). These data demonstrate that therapeutic delivery of miR-486-AAV9 shortly after myocardial reperfusion still has protective effects against cardiac I/R injury and cardiac dysfunction.

Increasing miR-486 inhibits cardiomyocyte apoptosis

Next, we isolated neonatal rat cardiomyocytes (NRCMs) and determined the functional role of miR-486 in cardiomyocytes *in vitro*. Consistent with reduced miR-486 expression in cardiac I/R injury, miR-486 was also found to be downregulated in an OGDR-induced apoptosis model of NRCMs *in vitro* (Figure 3A). After confirming

trichrome staining for cardiac fibrosis in mouse heart tissues (n = 5 for sham groups, n = 8–9 for I/R injury [IRI] groups). Scale bar, 100 μm. (F) RT-PCR for CTGF, Col1a1, Col3a1, and BNP expression in mouse heart tissues (n = 9–10). Data between two groups were compared by unpaired two-tailed Student's t test. Data among four groups were compared by two-way ANOVA followed by Tukey's *post hoc* test. *p < 0.05, **p < 0.01, ***p < 0.001.

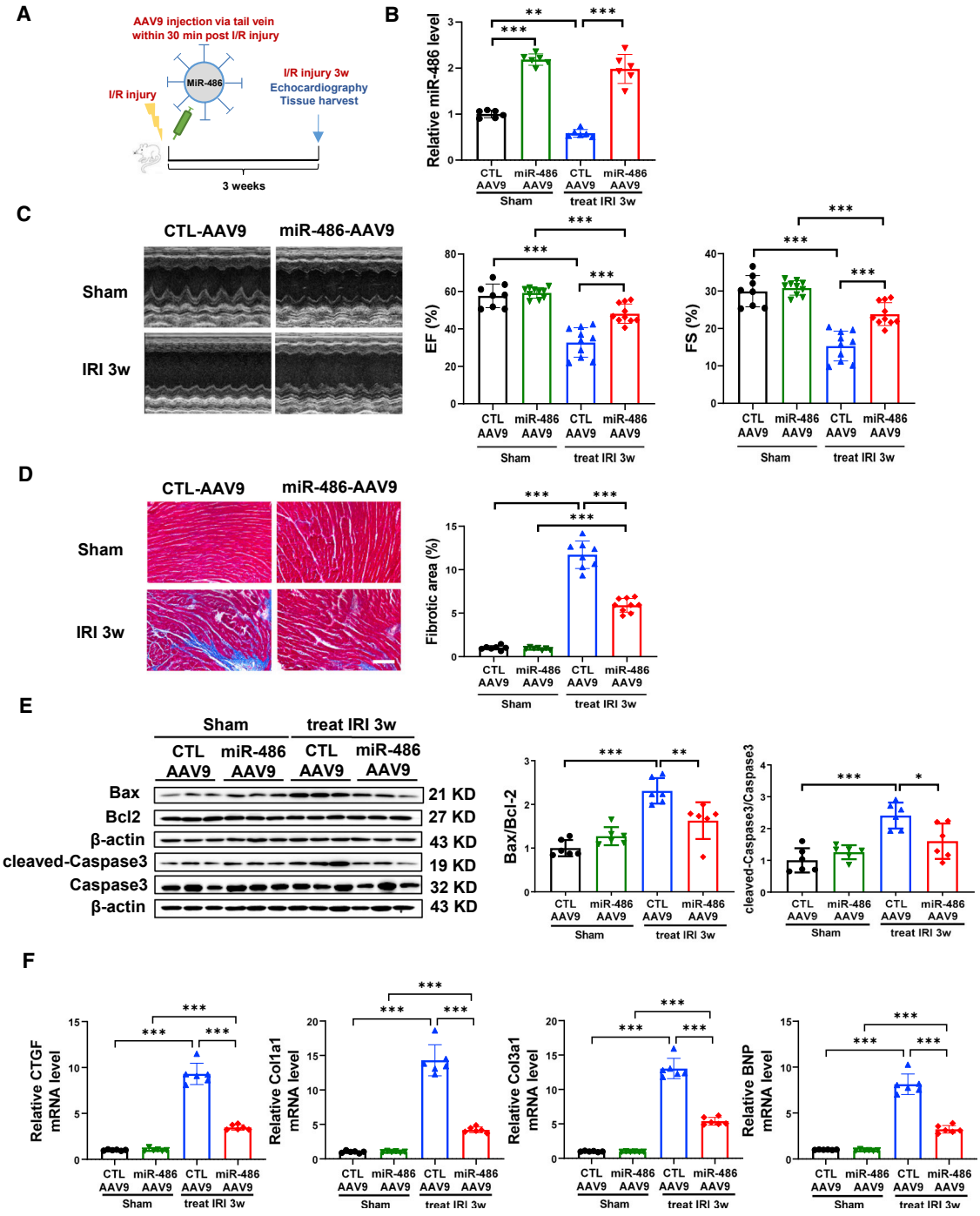

Figure 2. Therapeutic delivery of miR-486-AAV9 attenuates cardiac ischemia/reperfusion injury

(A) Schematic diagram showing that miR-486-AAV9 or CTL-AAV9 was injected via tail vein within 30 min of myocardial reperfusion, and echocardiography and tissue harvest were performed at 3 weeks post cardiac I/R injury. (B) RT-PCR for miR-486 expression in mouse heart tissues at 3 weeks post cardiac I/R injury (n = 6). (C) Echocardiography for left-ventricular ejection fraction (EF, %) and fractional shortening (FS, %) in mice at 3 weeks after I/R injury (n = 8–10). (D) Masson trichrome staining for cardiac fibrosis in mouse heart tissues (n = 7–9). Scale bar, 100 μm. (E) Western blot for Bax/Bcl-2 ratio and cleaved-caspase-3/caspase-3 ratio in mouse heart tissues (n = 6). (F) RT-PCR for CTGF, Col1a1, Col3a1, and BNP expression in mouse heart tissues (n = 6). Data were compared by two-way ANOVA followed by Tukey's *post hoc* test. *$p < 0.05$, **$p < 0.01$, ***$p < 0.001$.

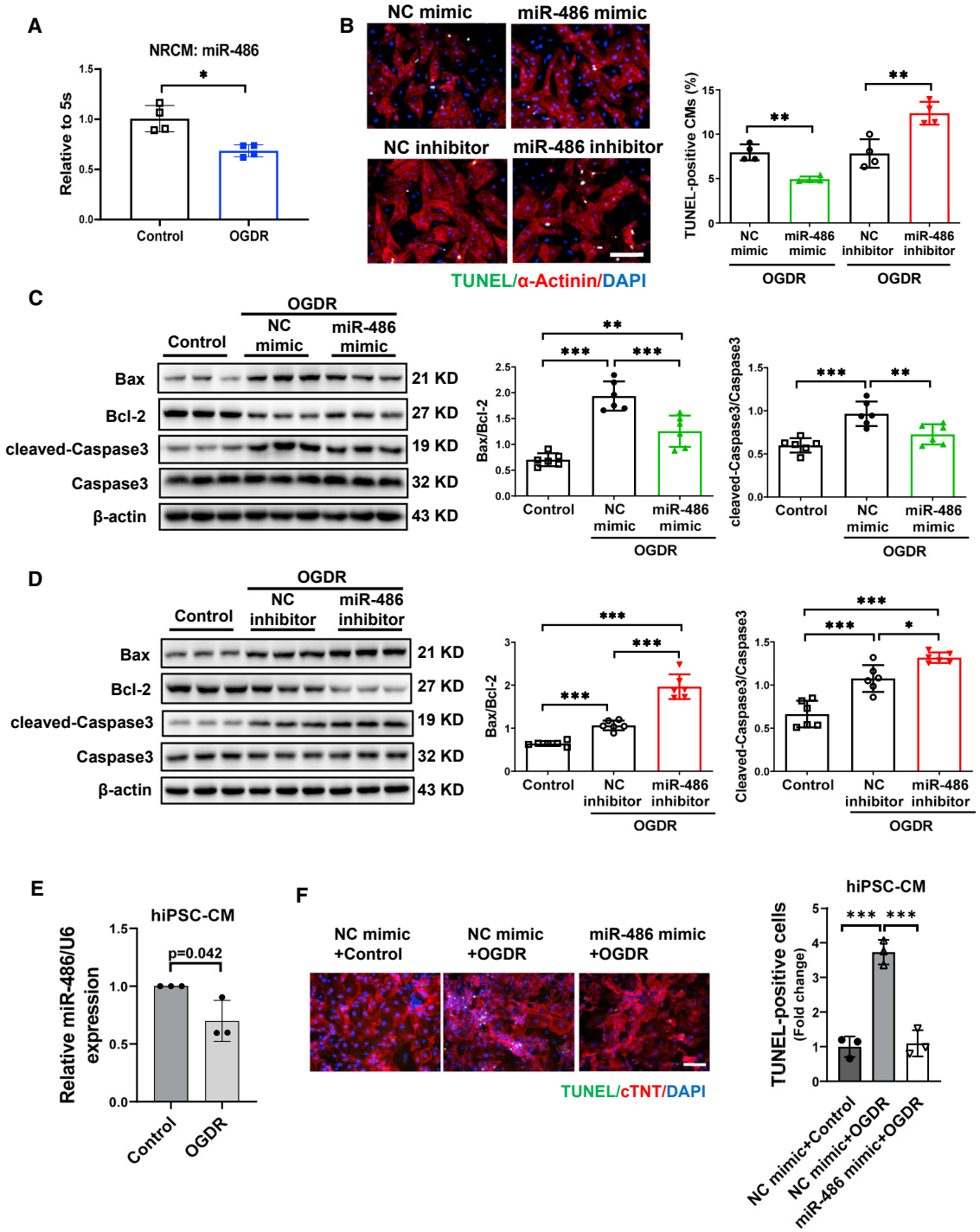

Figure 3. Overexpression of miR-486 inhibits cardiomyocyte apoptosis

(A) RT-PCR for miR-486 expression in primary cultured neonatal rat cardiomyocytes (NRCMs) treated with oxygen-glucose deprivation/reperfusion (OGDR) (n = 4). (B) TUNEL staining for α-actinin-labeled NRCMs transfected with miR-486 mimic, inhibitor, or negative control (NC) under OGDR stress (n = 4). Scale bar, 100 μm. (C and D) Western blot for Bax/Bcl-2 ratio and cleaved-caspase-3/caspase-3 ratio in OGDR-treated NRCMs transfected with miR-486 mimic (C), inhibitor (D), or negative controls (n = 6). (E) RT-PCR for miR-486 expression in human induced pluripotent stem cell-derived cardiomyocytes (hiPSC-CMs) treated with OGDR (n = 3). (F) TUNEL staining for cTnT-labeled human cardiomyocytes treated with OGDR (n = 3 technique repeats). Scale bar, 100 μm. Data between two groups were compared by unpaired two-tailed Student's t test. Data among three groups were compared by one-way ANOVA. *p < 0.05, **p < 0.01, ***p < 0.001.

that transfection of miR-486 mimic or inhibitor could efficiently regulate miR-486 expression in NRCMs (Figure S5A), we further examined OGDR-induced cardiomyocyte apoptosis using TUNEL staining and western blot for apoptosis-associated proteins. Our data showed that miR-486 mimic significantly reduced TUNEL-positive cardiomyocytes, while miR-486 inhibitor increased them (Figure 3B). Meanwhile, OGDR treatment caused elevated Bax/Bcl-2 ratio and cleaved-caspase-3/caspase-3 ratio at the protein level, which could be significantly reversed by miR-486 mimic (Figure 3C). On the other hand, miR-486 inhibitor transfection further increased Bax/Bcl-2 ratio and caspase-3 cleavage in OGDR-treated NRCMs (Figure 3D). These data provide direct evidence that increasing miR-486 exerts anti-apoptotic effects in cardiomyocytes.

To further test the potential role of miR-486 in human cardiomyocytes, we performed OGDR stress on human induced pluripotent stem cell-derived cardiomyocytes (hiPSC-CMs). The purity of the hiPSC-CMs was confirmed by cardiac troponin T (cTnT) immunofluorescence staining (Figure S5B). In line with downregulated expression in OGDR-treated NRCMs, miR-486 was also decreased in hiPSC-CMs with OGDR stress compared with controls (Figure 3E). Further, we efficiently transfected an miR-486 mimic into hiPSC-CMs (Figure S5C), and explored whether miR-486 overexpression could inhibit OGDR-induced apoptosis in human cardiomyocytes. Although the hiPSC-CM numbers were not significantly changed after OGDR stress (Figure S5D), OGDR increased the ratio of apoptotic hiPSC-CMs as demonstrated by TUNEL assay (Figure 3F). Interestingly, hiPSC-CMs overexpressing miR-486 showed clearly lower levels of apoptosis under OGDR stress compared with negative controls (Figure 3F), suggesting that myocardial protection by miR-486 is also conserved in human cardiomyocytes.

miR-486 targets PTEN and FoxO1 in cardiomyocytes

To identify the target genes of miR-486, we applied bioinformatic analysis using miRDB, Target Scan, and miRTarBase algorithms, and further subjected the predicted target genes of miR-486 in the Enrichr database. Among the common predicted target genes, PTEN and FoxO1 were critically involved in the pathways sorted by KEGG (Figures 4A and 4B). Although PTEN and FoxO1 were previously reported as target genes of miR-486 in various cancer cells and also in the heart,[6,19] whether they mediate the roles of miR-486 in myocardial apoptosis and I/R injury remained unclear. To confirm whether miR-486 directly targets PTEN and FoxO1, we constructed luciferase reporter plasmids containing 3′ untranslated region (3′ UTR) binding sequences or mutated sequences of PTEN and FoxO1. Co-transfection with miR-486 mimic and plasmids containing PTEN or FoxO1 3′ UTR binding sequences significantly decreased luciferase activity in 293T cells, while the reduction of luciferase activity was not present when the 3′ UTR binding site was mutated, indicating that miR-486 could directly target the 3′ UTR of PTEN or FoxO1 (Figures 4C and 4D). In NRCMs, we further observed that miR-486 mimic was effective in downregulating PTEN and FoxO1 at both mRNA and protein levels, while miR-486 inhibitor upregulated PTEN and FoxO1 expression (Figures 4E–4H). Meanwhile, we observed a trend toward downregulation of PTEN and a statistically significant downregulation of FoxO1 at the mRNA level in hiPSC-CMs transfected with miR-486 mimic (Figure S6). These results prove that miR-486 directly targets and negatively regulates PTEN and FoxO1 in cardiomyocytes.

miR-486 inhibits cardiomyocyte apoptosis by targeting PTEN and FoxO1

To further determine whether PTEN and FoxO1 mediate the functional role of miR-486 in cardiomyocytes, we performed co-transfection of miR-486 inhibitor with small interfering RNA (siRNA) targeting PTEN or FoxO1. We first confirmed that PTEN or FoxO1 siRNA transfection could significantly downregulate their expression in NRCMs (Figure S7). In NRCMs co-transfected with miR-486 inhibitor and PTEN siRNA, we observed that silencing PTEN was able to abolish the pro-apoptotic effect of miR-486 inhibitor in OGDR-treated cardiomyocytes as determined by TUNEL staining (Figure 5A) and western blot (Figure S8). Similarly, siRNA targeting FoxO1 also attenuated the deleterious effect of miR-486 inhibitor on cardiomyocyte apoptosis (Figures 5B and S9). Overexpressing PTEN or FoxO1 abolished the beneficial effect of miR-486 mimic in reducing cardiomyocyte apoptosis (Figure S10). Interestingly, both preventive and therapeutic delivery of miR-486-AAV9 were able to reduce PTEN and FoxO1 expression in mouse hearts both in the sham and in the I/R groups (Figures S11A, S11B, 5C, and 5D). These experiments indicate that PTEN and FoxO1 are critical target genes of miR-486 in regulating cardiomyocyte apoptosis, and provide *in vivo* evidence that miR-486 could modulate PTEN and FoxO1 in heart tissues under both normal and I/R injury conditions.

Anti-apoptotic effect of miR-486 is associated with AKT/mTOR activation

PTEN is well known for its inactivation effect on AKT signaling, which regulates cell growth and survival.[20] As PTEN functions as a target gene of miR-486 in cardiomyocytes, we further determined whether miR-486 could regulate AKT phosphorylation and subsequent mTOR activation. In NRCMs transfected with miR-486 mimic or inhibitor, we observed that miR-486 overexpression significantly increased AKT phosphorylation and induced mTOR and P70S6K activation (Figure 6A), while miR-486 inhibitor dampened the phosphorylation levels of the AKT/mTOR/P70S6K pathway (Figure 6B). Next, we co-treated NRCMs with miR-486 mimic and AKT inhibitor (MK2206) or mTOR inhibitor (rapamycin) in the condition of OGDR. As shown by TUNEL staining and western blot, AKT or mTOR inhibition was sufficient to attenuate the protective effect of miR-486 mimic against cardiomyocyte apoptosis (Figures 6C, 6D, and S12). Moreover, AAV9-mediated miR-486 overexpression was also sufficient to increase Akt phosphorylation levels in heart tissues suffering from I/R injury (Figures 6E and S11C). Collectively, these results highly suggest that miR-486 may target PTEN and subsequently activate AKT/mTOR pathways to protect against myocardial apoptosis.

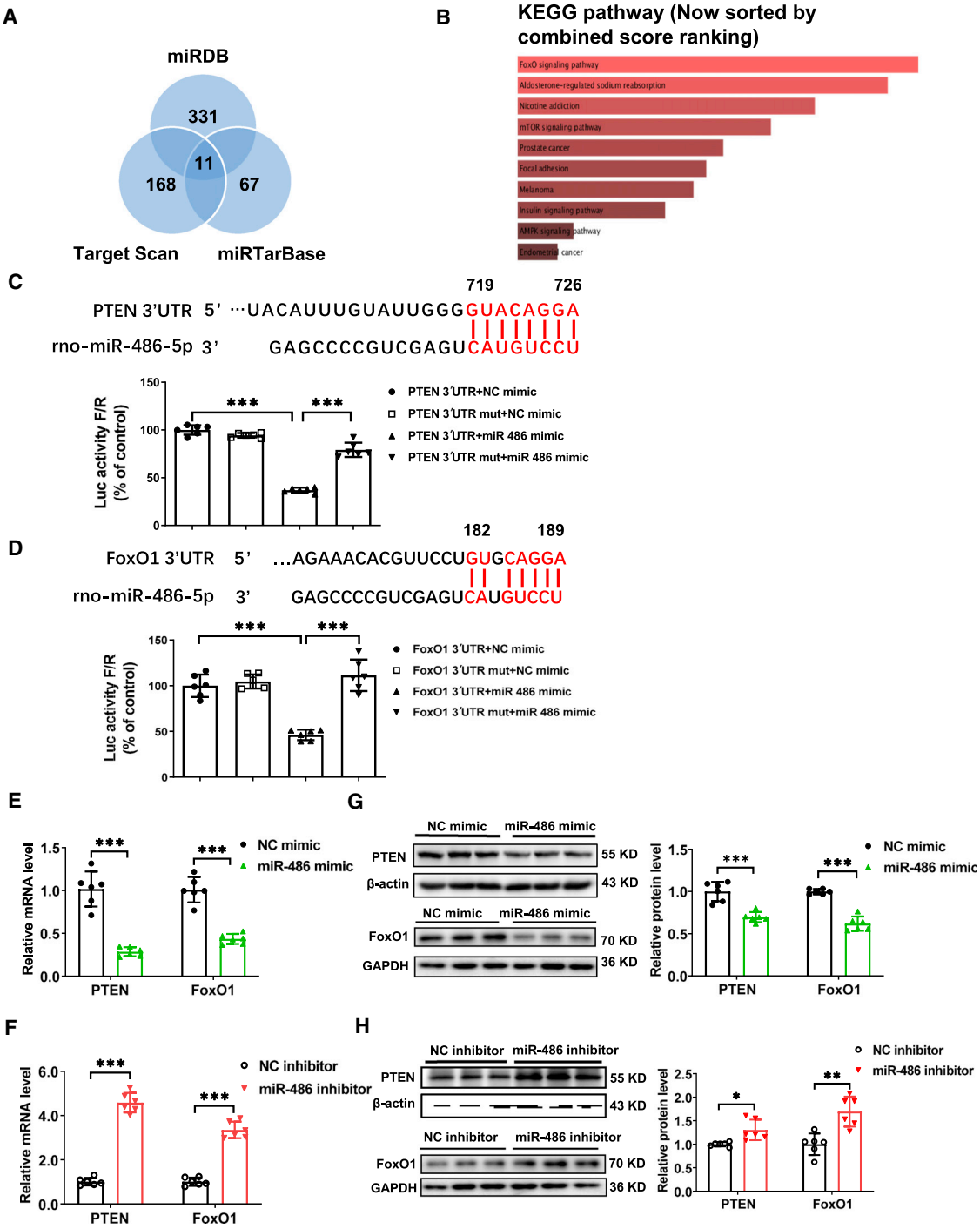

Figure 4. miR-486 targets PTEN and FoxO1 in cardiomyocytes

(A and B) Bioinformatic analysis using miRDB, Target Scan, and miRTarBase algorithms (A) and KEGG pathway analysis (B). (C and D) Luciferase reporter assays performed in 293T cells transfected with miR-486 mimic (or negative control, NC mimic) and luciferase reporter plasmids containing the binding sitein the 3′ UTR of PTEN (C, PTEN 3'UTR) or FoxO1 (D, FoxO1 3'UTR) or the mutated binding site in the 3'UTR of PTEN (C, PTEN 3'UTR mut) or FoxO1 (D, FoxO1 3'UTR mut) (n = 6). (E and F) RT-PCR for PTEN and FoxO1 expression in primary cultured neonatal rat cardiomyocytes (NRCMs) transfected with miR-486 mimic (E), inhibitor (F), or NC (n = 6). (G and H) Western blot for PTEN and FoxO1 expression in NRCMs transfected with miR-486 mimic (G), inhibitor (H), or NC (n = 6). Data between two groups were compared by unpaired two-tailed Student's t test. Data among four groups were compared by two-way ANOVA followed by Tukey's *post hoc* test. *p < 0.05, **p < 0.01, ***p < 0.001.

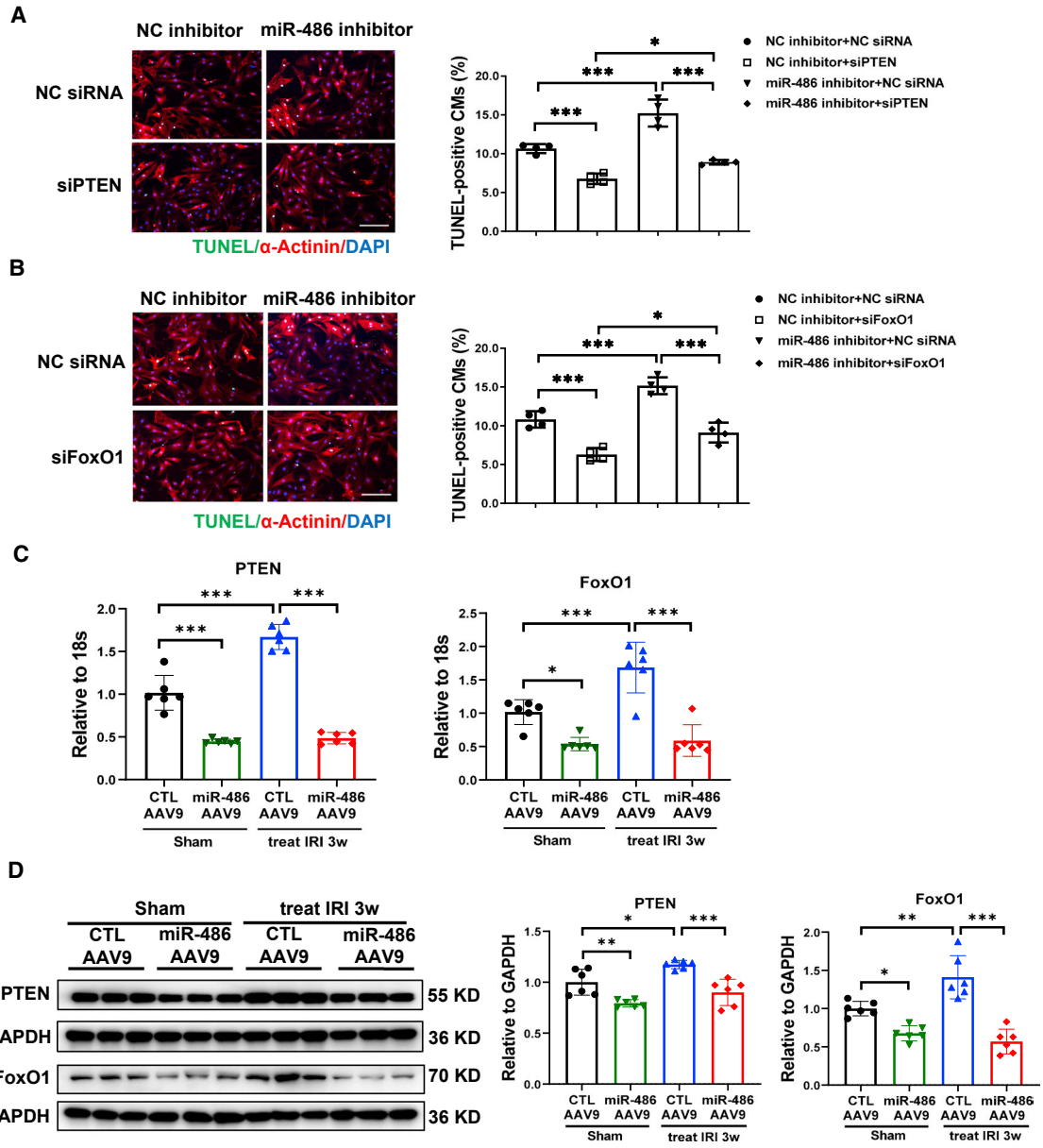

Figure 5. miR-486 inhibits cardiomyocyte apoptosis via targeting of PTEN and FoxO1

(A and B) TUNEL staining for α-actinin-labeled neonatal rat cardiomyocytes (NRCMs) transfected with miR-486 inhibitor and siRNA targeting PTEN (A) or FoxO1 (B) in the condition of oxygen glucose deprivation/reperfusion (OGDR) treatment (n = 4). Scale bar, 100 μm. (C and D) RT-PCR (C) and western blot (D) for PTEN and FoxO1 expression in heart tissues from mice treated with miR-486-AAV9 within 30 min of myocardial reperfusion. Heart tissues were harvested at 3 weeks post cardiac ischemia/reperfusion (I/R) injury (n = 6). Data were compared by two-way ANOVA followed by Tukey's *post hoc* test. *p < 0.05, **p < 0.01, ***p < 0.001.

Cardiomyocyte-specific overexpression of miR-486 alleviates cardiac I/R injury

miR-486 was previously reported to protect against tissue fibrosis, including myocardial interstitial fibrosis, through targeting of Smad1 and/or Smad2.[21] Interestingly, using isolated neonatal rat cardiac fibroblasts (NRCFs), we found that miR-486 mimic also inhibited NRCF proliferation and differentiation into myofibroblasts under stimulation of transforming growth factor β (TGF-β), while miR-486 inhibitor enhanced both NRCF proliferation and their differentiation into myofibroblasts regardless of TGF-β stimulation (Figure S13). Meanwhile, we demonstrated that miR-486 negatively regulated Smad1 and Smad2 at both mRNA and protein levels in NRCFs (Figure S14). These data indicate that miR-486 also has inhibitory effects on cardiac fibroblast proliferation and activation, which

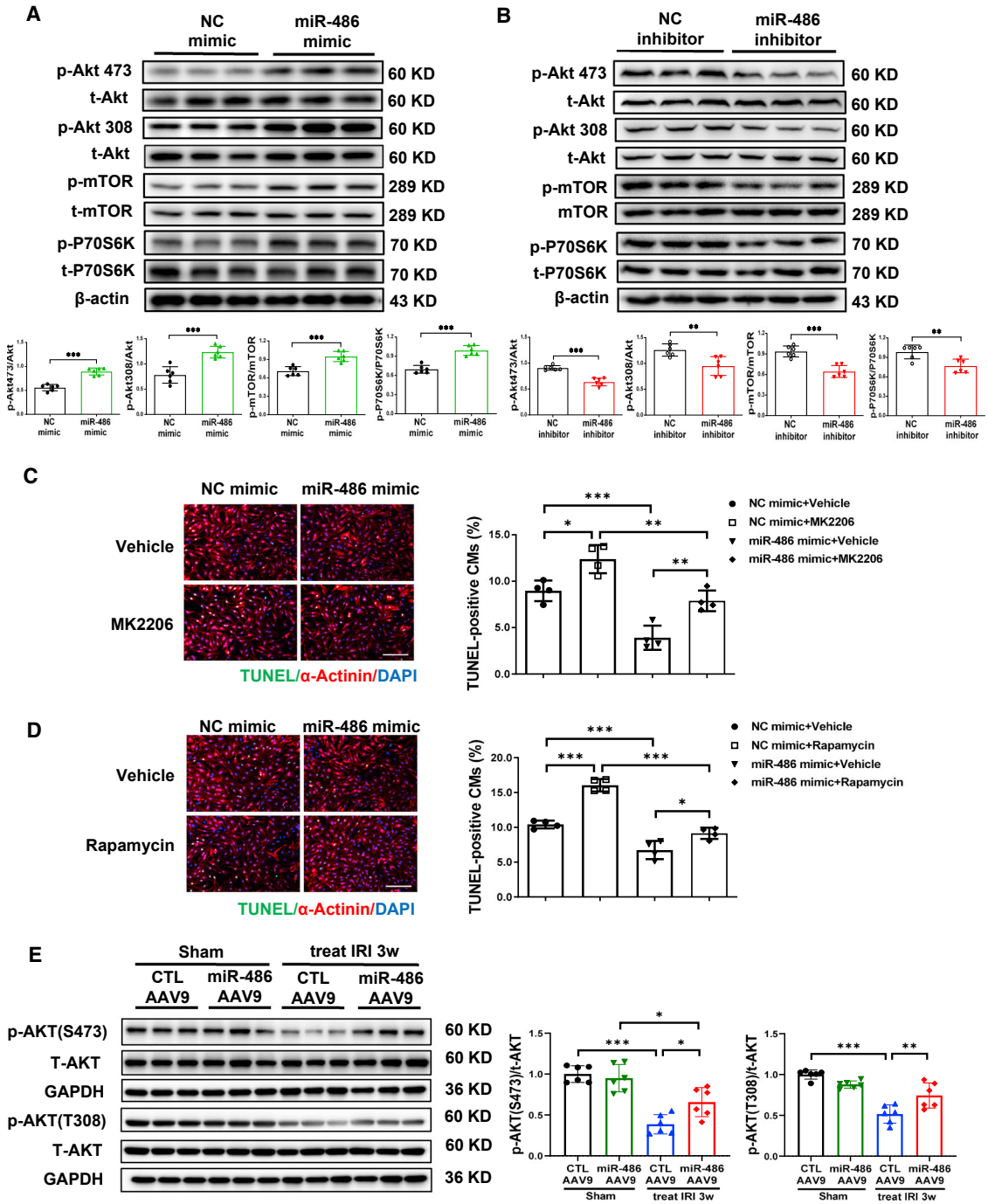

Figure 6. miR-486 inhibits cardiomyocyte apoptosis by activating the AKT/mTOR pathway

(A and B) Western blot for phosphorylation levels of the AKT/mTOR/P70S6K pathway in NRCMs transfected with miR-486 mimic (A), inhibitor (B), or negative controls (NC) (n = 6). (C and D) TUNEL staining for α-actinin-labeled NRCMs treated with miR-486 mimic and AKT inhibitor MK2206 (C) (n = 4) or mTOR inhibitor rapamycin (D) (n = 4). Scale bar, 100 μm. (E) Western blot for AKT phosphorylation levels in heart tissues from mice treated with miR-486-AAV9 within 30 min of myocardial reperfusion. Heart tissues were harvested at 3 weeks post cardiac ischemia/reperfusion (I/R) injury (n = 6). Data between two groups were compared by unpaired two-tailed Student's t test. Data among four groups were compared by two-way ANOVA followed by Tukey's *post hoc* test. *p < 0.05, **p < 0.01, ***p < 0.001.

may contribute to the beneficial effect of AAV9-mediated miR-486 overexpression in heart tissues against cardiac I/R injury.

Under these circumstances, we further constructed AAV9 expressing miR-486 with a cardiac muscle cell-specific promoter, cTnT (cTnT-miR-486 AAV9), to investigate whether overexpression of miR-486 in cardiomyocytes could be sufficient to protect against cardiac I/R injury. The therapeutic delivery of cTnT-miR-486 AAV9 was performed within 30 min of cardiac I/R injury (Figure 7A), and miR-486 was significantly increased in heart tissues from mice treated with cTnT-miR-486 AAV9 (Figure 7B). Meanwhile, immunofluorescence imaging showed an obvious co-localization of ZsGreen (indicative of AAV9) and α-actinin staining in heart tissues from mice injected with cTnT-miR-486 AAV9 or cTnT-control vectors (Figure S15A), supporting an efficient delivery of AAV9 in cardiomyocytes *in vivo*. We further demonstrated that cTnT-miR-486 AAV9 was able to attenuate cardiac dysfunction and cardiac fibrosis, and downregulated apoptosis- and fibrosis-associated proteins or gene markers at 3 weeks post I/R injury (Figures 7C–7F). Moreover, cTnT-miR-486 AAV9 significantly downregulated PTEN and FoxO1 expression (Figures S15B and S15C) and activated AKT phosphorylation (Figure S15D) in heart tissues. These data suggest that in addition to miR-486 overexpression in the whole heart, cardiomyocyte-targeted miR-486 overexpression is also effective at alleviating cardiac I/R injury in association with its myocardial protection effect through targeting of PTEN and FoxO1 and activation of AKT.

miR-486 is necessary for exercise-induced myocardial protection

miR-486 was previously reported to be induced in heart tissues after exercise training.[18] In the present study, we further examined the regulatory effect of exercise on miR-486 in a mouse model of regular swimming exercise. Here we observed that swimming exercise significantly induced miR-486 expression (Figure 8A), and also regulated known cardioprotective factors responsive to exercise, such as CITED4, miR-222, and lncRNA CPhar, in mouse heart tissues (Figure S16A). Specifically, miR-486 was increased in mouse isolated cardiomyocytes, but not in cardiac fibroblasts from swimming mouse hearts (Figure 8A). Meanwhile, we observed that miR-486 was upregulated in the serum samples as well as in the gastrocnemius and anterior tibialis from swimming mice (Figures S16B–S16D). These data suggest that a regular exercise training such as swimming is effective at inducing miR-486 expression, which prompted us to further investigate whether miR-486 is necessary to mediate the beneficial effect of exercise against cardiac I/R injury.

Mice were injected with miR-486 sponge AAV9 or CTL-AAV9 and then subjected to swimming exercise before cardiac I/R injury (Figure 8B). Our data showed a protective effect of exercise in reducing the infarct size upon acute I/R injury, which was, however, attenuated by miR-486 inhibition (Figure 8C). At 1 week after I/R injury, we confirmed that miR-486 sponge AAV9 significantly reduced exercise-induced miR-486 level in I/R hearts (Figure 8D). The protective effects of exercise against cardiac dysfunction, myocardial apoptosis, and cardiac remodeling were also abolished by miR-486 inhibition (Figures 8E–8G and S17A). Moreover, exercise training downregulated PTEN and FoxO1 in the heart, while miR-486 sponge AAV9 abolished these modulations (Figures 8G and S17B). Similarly, miR-486 knockout (KO) mice and wild-type (WT) littermates were subjected to swimming exercise before I/R injury (Figure S18A). We also observed that miR-486 KO swimming mice had significantly increased infarct size compared with WT swimming mice (Figure S18B). Collectively, these data suggest that miR-486 is necessary for exercise-induced myocardial protection upon I/R injury.

DISCUSSION

Exercise and its regulated molecules have myocardial protective effects and can protect against cardiac I/R injury.[22] miR-486, enriched in muscle, was previously identified to be upregulated in the heart after exercise training,[18] which prompted us to investigate the functional roles of miR-486 in cardiac I/R injury and to explore further the potential of miR-486 contributing to exercise-induced protection against I/R injury.

In the present study, a consistent downregulation of miR-486 was observed in both cardiac I/R injury *in vivo* and OGDR-treated cardiomyocytes *in vitro*. Functionally, AAV9-mediated miR-486 overexpression significantly prevented cardiac I/R injury *in vivo*, as evidenced by reduced infarct size in the acute-phase and preserved cardiac function at long term. Noteworthy, therapeutic delivery of miR-486-AAV9 shortly after myocardial reperfusion still exerted obvious protective effects against cardiac I/R injury and cardiac dysfunction, suggesting a practicable therapeutic intervention by increasing miR-486 in the treatment of cardiac I/R injury. Moreover, to specifically elucidate the functional role of miR-486 in myocardial protection, we treated mice with AAV9 expressing miR-486 with a cardiac muscle cell-specific promoter, cTnT, and found that cardiac muscle cell-targeted overexpression of miR-486 was still sufficient to protect against cardiac I/R injury *in vivo*. Collectively, these data provide strong evidence indicating that therapeutic miR-486 overexpression has myocardial protective effects against cardiac I/R injury.

Cardiomyocyte apoptosis is a critical pathological feature of I/R injury, which may further contribute to the development of cardiac remodeling and heart failure.[23] Our data further demonstrated that both preventive and therapeutic interventions of miR-486 overexpression *in vivo* could reduce myocardial apoptosis in I/R mice, and miR-486 also inhibited OGDR-induced apoptosis in primary cultured NRCMs *in vitro*. Previous studies reported that miR-486 reduced H_2O_2-induced apoptosis in H9C2 cells,[8] and prevented microembolization-induced myocardial apoptosis in rats.[9] miR-486 was also shown to mediate the protective effect of bone marrow stromal cell-derived exosomes and circulating extracellular vesicles against cardiac I/R injury.[10,24] Here we provide direct evidence that miR-486 overexpression is an efficient way to reduce cardiac I/R injury and cardiomyocyte apoptosis, as well as improving cardiac function at long term. Furthermore, we demonstrate that miR-486

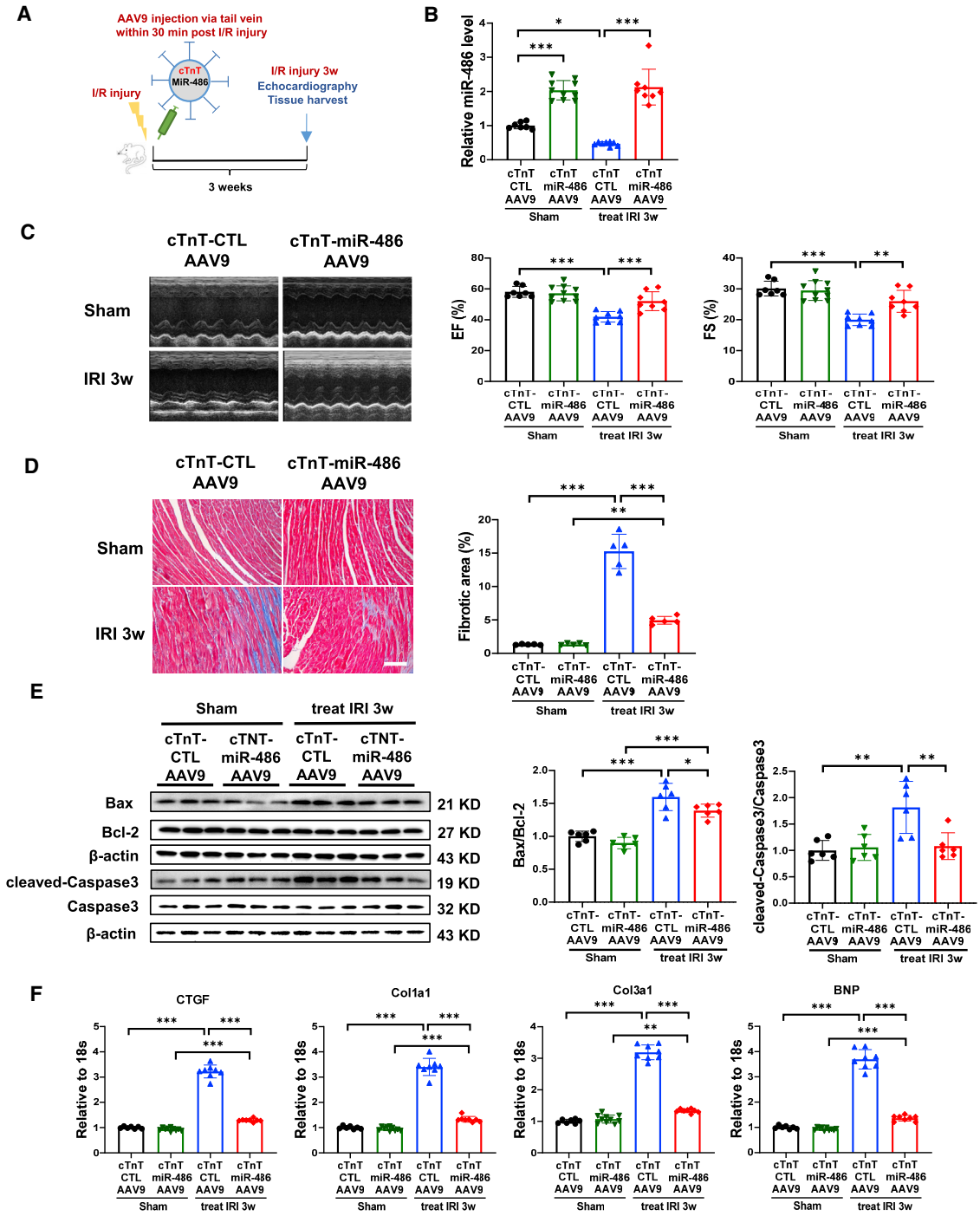

Figure 7. Cardiomyocyte-specific overexpression of miR-486 is a therapeutic to alleviate cardiac ischemia/reperfusion injury

(A) Schematic diagram showing that AAV9 expressing miR-486 with a cardiac muscle cell-specific promoter, cTnT (cTnT-miR-486 AAV9), or cTnT-CTL AAV9 was injected via the tail vein within 30 min of myocardial reperfusion, and echocardiography and tissue harvest were performed at 3 weeks post cardiac I/R injury. (B) RT-PCR for miR-486 expression in mouse heart tissues at 3 weeks post cardiac I/R injury (n = 7–10). (C) Echocardiography for left-ventricular ejection fraction (EF, %) and fractional shortening (FS, %) in mice at 3 weeks after I/R injury (n = 7–10). (D) Masson trichrome staining for cardiac fibrosis in mouse heart tissues (n = 5). Scale bar, 100 μm. (E) Western blot for Bax/Bcl-2 ratio and cleaved-caspase-3/caspase-3 ratio in mouse heart tissues (n = 6). (F) RT-PCR for CTGF, Col1a1, Col3a1, and BNP expression in mouse heart tissues (n = 7–10). Data were compared by two-way ANOVA followed by Tukey's *post hoc* test. *p < 0.05, **p < 0.01, ***p < 0.001.

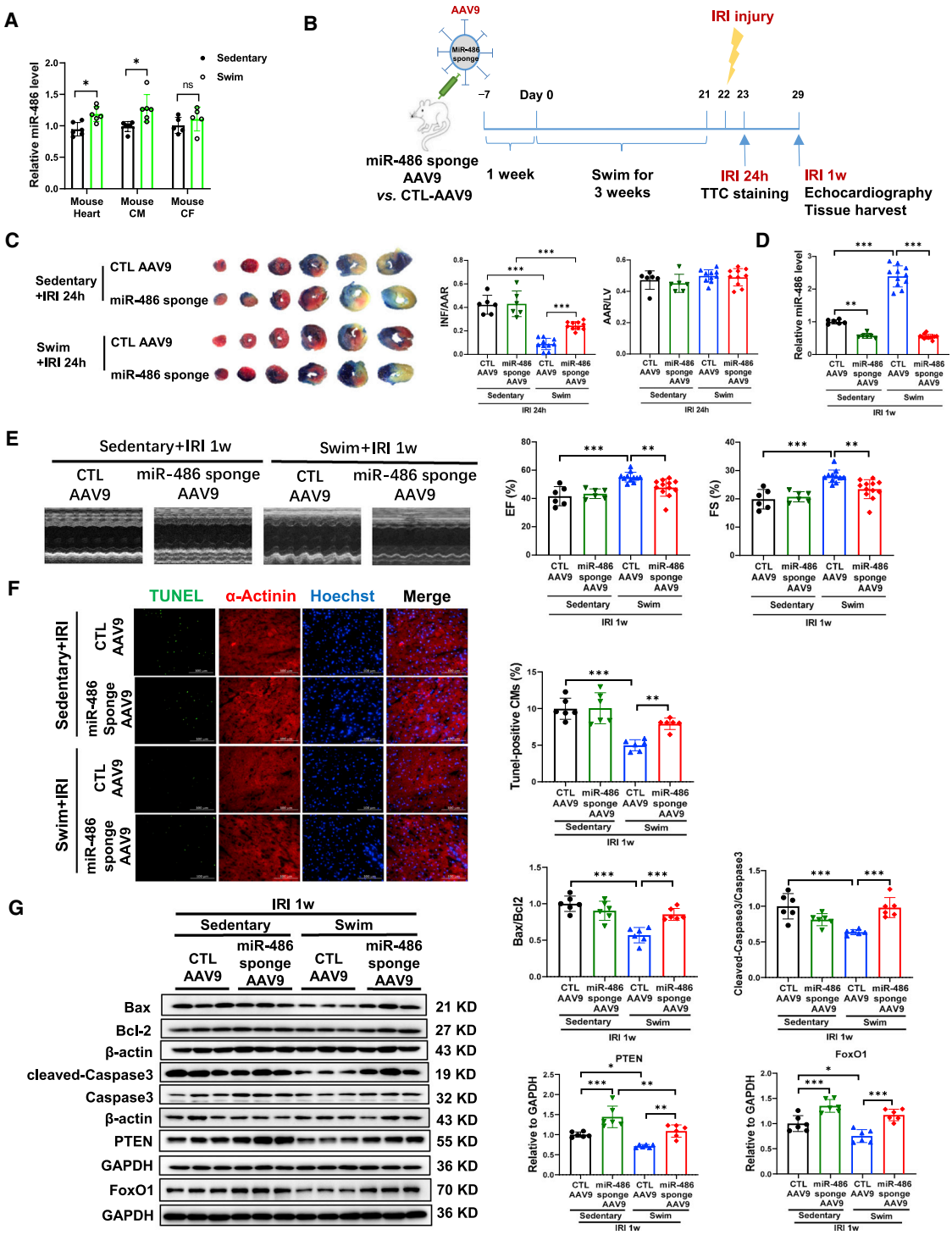

Figure 8. miR-486 is necessary for exercise-induced myocardial protection

(A) RT-PCR for miR-486 expression in the mouse heart and isolated mouse cardiomyocytes (CMs) or cardiac fibroblasts (CFs) from swimming or sedentary mice (n = 5–6). (B) Schematic diagram showing that mice were injected with miR-486 sponge AAV9 and then subjected to 3 weeks of swimming exercise before cardiac ischemia/reperfusion (I/R) injury. (C) The 2,3,5-triphenyltetrazolium chloride (TTC) staining for infarct size at 24 h after cardiac I/R injury as determined by the infarct-size/area-at-risk (INF/AAR) ratio. The area-at-risk/left-ventricle-weight (AAR/LV) ratio represents the homogeneity of surgery (n = 6 for sedentary mice, n = 10 for swimming mice). (D) RT-PCR for miR-486 expression in mouse heart tissues at 1 week post cardiac I/R injury (n = 6 for sedentary mice, n = 11–12 for swimming mice). (E) Echocardiography for left-ventricular ejection

(legend continued on next page)

also exerts anti-apoptotic effects in human cardiomyocytes, highlighting its potential effect in human myocardial protection.

miRNAs are known to function by binding to the 3′ UTR of target genes, which leads to mRNA degradation and/or translation inhibition.[25] Here we performed bioinformatic algorithms and identified that miR-486 directly interacted with the 3′ UTR of PTEN and FoxO1. PTEN was previously reported to be regulated by miR-486 in various cancer cell lines and also in the heart,[9,19] and increasing evidence has indicated that PTEN inactivation, which is associated with reduced apoptosis, prevents cardiac I/R injury.[26] However, whether PTEN mediates the role of miR-486 in myocardial apoptosis and I/R injury remained unclear. In addition, FoxO1 was identified as another target gene of miR-486,[6,27] although little was known about the functional relationship between miR-486 and FoxO1 in the heart. In the present study, we first observed that miR-486 negatively regulated PTEN and FoxO1 at both mRNA and protein levels in cardiomyocytes, and miR-486 overexpression led to downregulated PTEN and FoxO1 in the heart. We further showed that silencing PTEN or FoxO1 was able to rescue the pro-apoptotic effect of miR-486 inhibitor in cardiomyocytes, while overexpressing downstream targets abolished the effect of miR-486 in reducing cardiomyocyte apoptosis. These data indicate that PTEN and FoxO1 are direct targets of miR-486 in the regulation of myocardial apoptosis and I/R injury.

AKT/mTOR signaling is essentially involved in the regulation of cell growth and survival.[28] PTEN inactivation and subsequent activation of the AKT/mTOR pathway is a desirable means to promote cell survival while inhibiting apoptosis.[29,30] In line with the downregulation of PTEN, our data demonstrated that miR-486 overexpression led to an activation of the AKT/mTOR/P70S6K pathway in cardiomyocytes. On the other hand, the AKT/mTOR/P70S6K phosphorylation levels were significantly reduced in cardiomyocytes with miR-486 inhibition. Function rescue experiments further indicated that AKT and mTOR activation is necessary to mediate the protective effect of miR-486 against cardiomyocyte apoptosis. Interestingly, AKT activation in turn can lead to repression of FoxO1 activity, which is an important approach to prevent apoptosis.[31,32] In our study, we also observed that miR-486 overexpression was able to increase AKT phosphorylation levels in heart tissues from I/R mice, indicative of an *in vivo* activation of AKT by increasing miR-486 during cardiac I/R injury.

Mounting evidence has shown that exercise per se and exercise-regulated molecules can have myocardial protective effects against I/R injury and cardiac remodeling,[16,22] and miR-486 was previously identified to be upregulated in the heart after exercise training.[18] Swimming exercise has been previously demonstrated to be beneficial for myocardial protection.[17] In the present study, we demonstrated that miR-486 was significantly upregulated in the heart tissues and serum samples after swimming exercise. Next, we injected mice with miR-486 sponge AAV9 and then subjected mice to swimming exercise before cardiac I/R injury. Interestingly, we observed that miR-486 inhibition significantly attenuated the beneficial effect of exercise against cardiac I/R injury, myocardial apoptosis, and cardiac dysfunction. Swimming exercise led to downregulated PTEN and FoxO1 in the I/R hearts, which was, however, reversed by miR-486 inhibition. We further demonstrated that swimming-exercised mice with miR-486 KO had significantly increased infarct size after I/R injury compared with WT exercised mice. These data consistently indicate that miR-486 is necessary for the myocardial protective effect of exercise against cardiac I/R injury.

In conclusion, miR-486 is protective against cardiac I/R injury and myocardial apoptosis through the targeting of PTEN and FoxO1 and activation of the AKT/mTOR pathway, and mediates the beneficial effect of exercise for myocardial protection (see the graphical abstract). With the encouraging development of non-coding RNA-based therapeutics, increasing miR-486 might be a promising therapeutic strategy for myocardial protection.

MATERIALS AND METHODS

Animals and cardiac I/R injury model

Male C57BL/6J mice ages 8–10 weeks were purchased from Cavens Lab Animal (Changzhou, China) and maintained in the specific-pathogen-free (SPF) laboratory animal facility of Shanghai University (Shanghai, China). miR-486 KO mice were generated using CRISPR-Cas9-mediated genome engineering by VIEWSOLID BIOTECH (Beijing, China). Briefly, guide RNA (gRNA) targeting vectors were constructed based on the mature sequence of mmu-miR-486 on mouse chromosome 8. The Cas9 mRNA and validated gRNA generated by *in vitro* transcription were co-injected into fertilized eggs for KO mouse production. The pups were genotyped by PCR followed by sequence analysis, which showed a deletion of 254 bp containing the mature sequence of miR-486. All animal experiments were conducted in accordance with the *Guidelines for the Care and Use of Laboratory Animals* for biomedical research published by the National Institutes of Health (No. 85-23, revised 1996) and approved by the Committee for the Ethics of Animal Experiments of Shanghai University. To induce acute cardiac I/R injury, mice were anesthetized with 4% chloral hydrate (intraperitoneally [i.p.], 10 μL/g body weight) followed by endotracheal ventilation, and the left anterior descending (LAD) coronary artery was ligated for 30 min and then reperfused for 24 h as previously reported.[18,23] Sham mice were subjected to the same surgery procedures, but without LAD ligation.

To study the preventive effect of miR-486 *in vivo*, AAV9 expressing miR-486 (miR-486-AAV9) was injected via the tail vein at a dose of 10^{11} virus genomes (v.g.) per mouse. miR-486-AAV9 and control

fraction (EF, %) and fractional shortening (FS, %) in mice at 1 week after I/R injury (n = 6 for sedentary mice, n = 11–12 for swimming mice). (F) TUNEL staining for myocardial apoptosis in α-actinin-labeled cardiomyocytes (n = 6). Scale bar, 100 μm. (G) Western blot for Bax/Bcl-2 ratio, cleaved-caspase-3/caspase-3 ratio, PTEN, and FoxO1 in mouse heart tissues (n = 6). Data between two groups were compared by unpaired two-tailed Student's t test. Data among four groups were compared by two-way ANOVA followed by Tukey's *post hoc* test. *p < 0.05, **p < 0.01, ***p < 0.001.

vectors (CTL-AAV9) were purchased from Hanbio Biotechnology (Shanghai, China). Briefly, the mmu-miR-486a-5p was inserted between the BamHI and the EcoRI restriction enzyme sites of the pHBAAV9-CMV-MCS-WPRE vector (Hanbio Biotechnology). AAVs were generated using packaging plasmids pAAV-rep/cap vector and pHelper vector together with AAV9-CMV-mmu-miR-486a-5p constructs. Three weeks after AAV9 injections, acute cardiac I/R injury was induced as described above. At 24 h after I/R injury, 2,3,5-triphenyltetrazolium chloride (TTC) staining and heart tissue harvest were performed. In another set of animal experiments, we constructed miR-486 sponge AAV9 and injected mice with miR-486 sponge AAV9 or control vectors via the tail vein at a dose of 10^{11} v.g. per mouse to investigate whether miR-486 inhibition could further aggravate cardiac I/R injury. The infarct size was measured using TTC staining at 24 h after I/R injury, and heart tissues were harvested for further examination. To study the effect of miR-486 on cardiac I/R injury in the long term, mice were injected with miR-486-AAV9 as described above, and 1 week later subjected to cardiac I/R injury. At 3 and 6 weeks after injury, echocardiography and heart tissue harvest were performed.

To study the potential therapeutic effect of miR-486 overexpression in cardiac I/R injury, mice were injected with miR-486-AAV9, AAV9 expressing miR-486 with the cardiac muscle cell-specific promoter cTnT (cTnT-miR-486 AAV9) (Hanbio Biotechnology), or control vectors at a dose of 10^{11} v.g. per mouse, within 30 min of cardiac I/R injury. Echocardiography and heart tissue harvest were performed after 3 weeks of I/R injury.

Swimming exercise training

To establish the mouse model of swimming exercise, mice were adapted to 5 min swimming in the morning and in the afternoon before formal exercise training. At the first day of swimming training, mice swam for 10 min twice a day, and the swimming time increased by 10 min each day until 90 min twice a day as previously reported.[17,18] After 4 weeks of swimming exercise, miR-486 expression levels were determined in mouse heart tissues, gastrocnemius and anterior tibialis muscles, and serum samples, as well as in the isolated cardiomyocytes and cardiac fibroblasts from adult swimming mice or sedentary mice as previously described.[16] To investigate the role of miR-486 in exercise-induced protection against cardiac I/R injury, mice were injected with miR-486 sponge AAV9 or CTL-AAV9 at 1 week before swimming, and then subjected to swimming exercise. After 3 weeks of swimming exercise, cardiac I/R injury was induced by LAD ligation and reperfusion as described above. Finally, TTC staining was performed to evaluate the infarct size at 24 h after I/R injury, and heart tissue harvest was performed at 1 week post I/R injury. In addition, 8- to 10-week-old male miR-486 KO mice and WT littermates received swimming exercise for 3 weeks and then were subjected to cardiac I/R injury for determination of the infarct size using TTC staining at 24 h after I/R injury.

TTC staining

At 24 h after cardiac I/R injury, mice were anesthetized with 4% chloral hydrate (i.p., 10 μL/g body weight) before the left ventricle was injected with 1 mL of 1% Evans blue. The heart was then sliced into 1-mm-thick tissue sections and stained with 1% TTC. The area-at-risk to left-ventricle-weight ratio (AAR/LV) was used to confirm homogeneity of surgery. The infarct-size to area-at-risk ratio (INF/AAR) was used to evaluate cardiac I/R injury.

Echocardiography for cardiac function

Mice were anesthetized with inhaled isoflurane and evaluated for cardiac function using echocardiography (FUJIFILM Visual Sonics). Left-ventricular ejection fraction (EF, %) and fractional shortening (FS, %) were measured and calculated through three consecutive cardiac cycles based on M-mode long-axis view of the left ventricle at the papillary muscle level.

Primary culture and treatment of neonatal rat cardiomyocytes and cardiac fibroblasts

NRCMs and NRCFs were isolated from 1- to 3-day-old Sprague-Dawley rats using collagenase II (Gibco, 17101015)/pancreatin from porcine pancreas (Sigma, P3292) digestion and Percoll (GE Healthcare, 17-0891-01) centrifugation protocol.[17,18] NRCMs were maintained in Dulbecco's modified Eagle's medium (DMEM, Corning) containing 4.5 g/L glucose supplemented with 10% horse serum (Gibco) and 5% fetal bovine serum (BioInd, Israel). To mimic cardiac I/R injury *in vitro*, NRCMs were treated with oxygen-glucose deprivation for 8 h followed by reperfusion for 12 h as previously described.[23] To study the functional role of miR-486 in OGDR-induced cardiomyocyte apoptosis, NRCMs were transfected with miR-486 mimic (50 nM), inhibitor (100 nM), or negative controls (RiboBio, Guangzhou, China) for 48 h using Lipofectamine 2000 (Invitrogen). Transfection of siRNAs targeting PTEN or FoxO1 (75 nM, RiboBio, Guangzhou, China), or plasmids expressing PTEN or FoxO1, was conducted in OGDR-treated NRCMs for 48 h to investigate the target genes of miR-486 in regulating cardiomyocyte apoptosis. Moreover, NRCMs were treated with the AKT inhibitor MK2206 (10 nM, Selleck) or mTOR inhibitor rapamycin (100 nM, Sigma) for 24 h under OGDR stress to elucidate whether AKT/mTOR activation was involved in the functional role of miR-486 in cardiomyocytes. NRCFs were maintained in DMEM (Corning) containing 4.5 g/L glucose supplemented with 10% fetal bovine serum. The functional roles of miR-486 were determined in NRCFs transfected with miR-486 mimic (50 nM) or inhibitor (100 nM) under stimulation of recombinant human TGF-β (Peprotech, Rocky Hill, NJ, USA) at 20 ng/mL for 48 h.

hiPSC-derived cardiomyocytes and treatment

The hiPSCs (hHSC_Iso4_ADCF_SeV-iPS2; alternative name, MHHi001) were reprogrammed from CD34-positive human cord blood hematopoietic stem cells of a healthy female donor as previously published.[33] Informed consent was obtained, in accordance with local regulations and Institutional Review Board requirements. The hiPSCs were maintained under feeder-free culture conditions using Geltrex (Thermo Scientific)-coated polystyrene plates (Greiner CELLSTAR) and StemMACS full medium with supplements (Milteny).[33] Directed differentiation of hiPSCs toward mesodermal

lineage was performed as described previously,[34] followed by a metabolic selection process to obtain a purified population of hiPSC-CMs.[35] hiPSC-CMs were maintained as described previously,[36] and transfected with 100 nM pre-miR hsa-miR-486 (AM17100) for 48 h and further put under OGDR stress. For OGDR stress, hiPSC-CMs were placed in a 1% O_2 incubator for 8 h with no glucose medium (supplemented with lactate). Then, the cells recovered in a 21% O_2 incubator for 12 h in normal maintenance medium. hiPSC-CMs transfected with pre-miR negative control 2 (Ambion, AM17111) served as controls. At the endpoint, TUNEL assays were performed to measure cell apoptosis.

Immunofluorescence staining

Cardiomyocyte apoptosis was examined using a TUNEL FITC apoptosis detection kit (Vazyme) according to the manufacturer's manuals. Briefly, frozen heart tissue sections or cultured cardiomyocytes were fixed with 4% paraformaldehyde (PFA) and permeabilized with 0.5% Triton X-100 before being blocked with 5% bovine serum albumin (BSA) for 1 h. Heart tissue sections or NRCMs were incubated with a 1:200 dilution of mouse anti-α-actinin (Sigma, A7811) at 4°C overnight, and then incubated with Cy3-AffiniPure goat anti-mouse IgG (H + L) (The Jackson Laboratory) for 1 h at room temperature. For hiPSC-CMs, cardiomyocytes were immunofluorescently labeled with cTnT (Thermo, MS-295-P0). Finally, heart tissue sections or cardiomyocytes were stained with the TUNEL FITC apoptosis detection kit (Vazyme) according to the manufacturer's instructions, and nuclei were counterstained with DAPI or Hoechst. A total of at least 10 fields per tissue or per well were photographed and analyzed using a confocal microscope (Carl Zeiss). The percentage of TUNEL-positive cardiomyocytes was determined to evaluate cardiomyocyte apoptosis upon cardiac I/R injury or OGDR stress. For immunofluorescence staining of α-SMA and EdU, NRCFs were pre-incubated with EdU working solution for 24 h and incubated with α-SMA-Cy3 antibody (Sigma, C6198) overnight at 4°C. EdU labeling was performed using the Click-iT Plus EdU Alexa Fluor 488 Imaging Kit (Invitrogen) according to the manufacturer's instructions, and nuclei were counterstained with Hoechst. A total of at least 10 fields per well were viewed under a confocal microscope (Carl Zeiss). The percentage of EdU-positive NRCFs and the immunofluorescence intensity of α-SMA were determined to evaluate cardiac fibroblast proliferation and differentiation to myofibroblasts.

Masson's trichrome staining

Heart tissues were embedded in paraffin, and 5-μm-thick sections were stained with Masson's trichrome (Solarbio, G1340) according to the manufacturer's manual. The percentage of fibrotic area to total area was evaluated for cardiac fibrosis. Images were analyzed using ImageJ software 1.50i (NIH, USA).

Luciferase reporter assay

To study the direct interaction between miR-486 and the 3′ UTR of PTEN and FoxO1, we constructed the luciferase reporter vector pGL3-Basic (Promega) containing the binding site (or mutated) with miR-486 in the 3′ UTR of PTEN (719–726) or FoxO1 (182–189). 293T cells were transfected with WT or mutated (mut) luciferase reporter plasmid with miR-486 mimic or negative control. The dual-luciferase reporter assay (Promega) was performed according to the manufacturer's instructions to study the direct binding of miR-486 in the 3′ UTR of PTEN or FoxO1 as determined by firefly/*Renilla* luciferase activity. To verify that miR-486 sponge was sufficient to target and bind miR-486, we constructed luciferase reporter vector pGL3-Basic (Promega) containing multiple tandem binding sites for miR-486. 293T cells were co-transfected with the miR-486 binding site-carrying luciferase reporter plasmids and the negative control (NC) mimic, miR-486 mimic, or miR-210 mimic. The group co-transfected with miR-210 mimic was designed to confirm that miR-486 had no binding activity with other miRNAs. Dual-luciferase reporter assay (Promega) was performed according to the manufacturer's instructions.

Real-time PCR

Total RNA was isolated from tissues or cultured cells using Trizol RNAiso Plus (TaKaRa). RNA concentration and quality were measured by NanoDrop (Thermo Scientific). A total of 100–400 ng RNA was then reverse transcribed to cDNA using a RevertAid First Strand cDNA synthesis kit (Thermo Scientific K1622). Real-time PCR was conducted using TaKaRa SYBR Premix Ex Taq (Tli RNaseH Plus, Japan) on a Roche LightCycler 480 PCR system. The primers for genes (forward and reverse 5′-3′) are listed in Table S1. For miRNA quantification in murine tissues and/or cells, real-time PCR was performed using a Bulge-Loop miRNA qRT-PCR primer set for miRNA (RiboBio, Guangzhou, China). 18s (or GAPDH) and 5s were used as internal controls for normal gene and miRNA, respectively. For quantification of miR-486 in mouse serum samples, total RNA was isolated using the MirVana miRNA isolation kit (Thermo Scientific, AM1561). *Caenorhabditis elegans* miR-39 (cel-miR-39) was added as the spike-in control. TaqMan assay (Thermo Fisher) was applied to measure miR-486-5p (assay 001278) expression in hiPSC-CMs, and U6 (assay 001973) was used as an internal control.

Western blotting

Total protein was lysed from heart tissues or cultured cells with RIPA lysis buffer (KeyGEN BioTECH, China) complemented with 1% phenylmethylsulfonyl fluoride (PMSF) and Pierce protease and phosphatase inhibitor (Thermo Scientific, 88668). Equal quantities of total protein were loaded on SDS-PAGE gels and transferred to PVDF membranes. Protein blots were blocked with 5% milk and incubated with primary antibodies for Bax (Abclonal, A0207), Bcl-2 (Abclonal, A2845), caspase-3 (Cell Signaling, 9662), PTEN (Cell Signaling, 9552), FoxO1 (Proteintech, 18592-1-AP), p-AKT 473 (Cell Signaling, 4051), p-AKT 308 (Cell Signaling, 2965), p-mTOR (Cell Signaling, 2971), p-P70S6K (Cell Signaling, 9205), Smad1 (Abclonal, A1101), and Smad2 (Abclonal, A19114) at 4°C overnight. Corresponding secondary antibodies were incubated on the next day before detection for protein bands using an enhanced chemiluminescence (ECL) kit. For phosphorylated proteins, protein blots were stripped and reblotted with specific antibodies for corresponding total protein, including AKT (Proteintech, 10176-2-AP), mTOR (Cell Signaling, 2972), and

P70S6K (Cell Signaling, 9202). GAPDH or β-actin was used as an internal control. Finally, protein band intensity was analyzed using ImageJ software.

Statistical analysis

All data were analyzed using SPSS software version 20.0 or GraphPad Prism 8. Experimental data were presented as the mean ± SD using GraphPad Prism 8. Data between two groups were compared by unpaired two-tailed Student's t test. Data among three groups were compared by one-way ANOVA. For more than three groups, data were compared by two-way ANOVA followed by Tukey's *post hoc* test. A $p < 0.05$ was considered statistically significant.

SUPPLEMENTAL INFORMATION

Supplemental information can be found online at https://doi.org/10.1016/j.ymthe.2022.01.031.

ACKNOWLEDGMENTS

This work was supported by grants from the National Key Research and Development Project (2018YFE0113500 to J.J.X.), National Natural Science Foundation of China (82020108002 and 81911540486 to J.J.X., 81770401 and 81970335 to Y.H.B.), Innovation Program of Shanghai Municipal Education Commission (2017-01-07-00-09-E00042 to J.J.X.), Science and Technology Commission of Shanghai Municipality (21XD1421300 and 20DZ2255400 to J.J.X.), "Dawn" Program of Shanghai Education Commission (19SG34 to J.J.X.), Shanghai Rising-Star Program (19QA1403900 to Y.H.B.), and Shanghai Committee of Science and Technology (21SQBS00100 to Y.H.B.). C.B. and T.T. received funding from the German Research Foundation, DFG (SFB/Transregio TRR267).

AUTHOR CONTRIBUTIONS

J.J.X. and T.T. designed the study, supervised all experiments, and drafted the manuscript. Y.H.B., D.C.L., and C.B. performed the experiments and analyzed the data. Y.J.Z., Z.Z.H., and M.Y.H. analyzed miR-486 in the murine model of swimming exercise. M.W., P.J.Y., S.Y.L., and K.W. established murine models of myocardial injury. S.C., A.C., I.R., and F.C.M. provided hiPSC-CMs and technical assistance. All authors read and approved the final manuscript.

DECLARATION OF INTERESTS

T.T. is a founder and shareholder of Cardior Pharmaceuticals GmbH. T.T. has filed and licensed patents on non-coding RNAs (outside of this work). The other authors declare no competing interests.

REFERENCES

1. Ibanez, B., Heusch, G., Ovize, M., and Van de Werf, F. (2015). Evolving therapies for myocardial ischemia/reperfusion injury. J. Am. Coll. Cardiol. *65*, 1454–1471.
2. Hausenloy, D.J., and Yellon, D.M. (2013). Myocardial ischemia-reperfusion injury: a neglected therapeutic target. J. Clin. Invest. *123*, 92–100.
3. Heusch, G., Libby, P., Gersh, B., Yellon, D., Bohm, M., Lopaschuk, G., and Opie, L. (2014). Cardiovascular remodelling in coronary artery disease and heart failure. Lancet *383*, 1933–1943.
4. Heusch, G., and Gersh, B.J. (2017). The pathophysiology of acute myocardial infarction and strategies of protection beyond reperfusion: a continual challenge. Eur. Heart J. *38*, 774–784.
5. Beermann, J., Piccoli, M.T., Viereck, J., and Thum, T. (2016). Non-coding RNAs in development and disease: background, mechanisms, and therapeutic approaches. Physiol. Rev. *96*, 1297–1325.
6. Small, E.M., O'Rourke, J.R., Moresi, V., Sutherland, L.B., McAnally, J., Gerard, R.D., Richardson, J.A., and Olson, E.N. (2010). Regulation of PI3-kinase/Akt signaling by muscle-enriched microRNA-486. Proc. Natl. Acad. Sci. U S A *107*, 4218–4223.
7. Chistiakov, D.A., Orekhov, A.N., and Bobryshev, Y.V. (2016). Cardiac-specific miRNA in cardiogenesis, heart function, and cardiac pathology (with focus on myocardial infarction). J. Mol. Cell Cardiol. *94*, 107–121.
8. Sun, Y., Su, Q., Li, L., Wang, X., Lu, Y., and Liang, J. (2017). MiR-486 regulates cardiomyocyte apoptosis by p53-mediated BCL-2 associated mitochondrial apoptotic pathway. BMC Cardiovasc. Disord. *17*, 119.
9. Zhu, H.H., Wang, X.T., Sun, Y.H., He, W.K., Liang, J.B., Mo, B.H., and Li, L. (2019). MicroRNA-486-5p targeting PTEN protects against coronary microembolization-induced cardiomyocyte apoptosis in rats by activating the PI3K/AKT pathway. Eur. J. Pharmacol. *855*, 244–251.
10. Wang, H., Maimaitiaili, R., Yao, J., Xie, Y., Qiang, S., Hu, F., Li, X., Shi, C., Jia, P., Yang, H., et al. (2021). Percutaneous intracoronary delivery of plasma extracellular vesicles protects the myocardium against ischemia-reperfusion injury in Canis. Hypertension *78*, 1541–1554.
11. McMullen, J.R., Amirahmadi, F., Woodcock, E.A., Schinke-Braun, M., Bouwman, R.D., Hewitt, K.A., Mollica, J.P., Zhang, L., Zhang, Y., Shioi, T., et al. (2007). Protective effects of exercise and phosphoinositide 3-kinase(p110alpha) signaling in dilated and hypertrophic cardiomyopathy. Proc. Natl. Acad. Sci. U S A *104*, 612–617.
12. Bei, Y., Zhou, Q., Sun, Q., and Xiao, J. (2015). Exercise as a platform for pharmacotherapy development in cardiac diseases. Curr. Pharm. Des. *21*, 4409–4416.
13. Bei, Y., Fu, S., Chen, X., Chen, M., Zhou, Q., Yu, P., Yao, J., Wang, H., Che, L., Xu, J., et al. (2017). Cardiac cell proliferation is not necessary for exercise-induced cardiac growth but required for its protection against ischaemia/reperfusion injury. J. Cell Mol. Med. *21*, 1648–1655.
14. Bostrom, P., Mann, N., Wu, J., Quintero, P.A., Plovie, E.R., Panakova, D., Gupta, R.K., Xiao, C., MacRae, C.A., Rosenzweig, A., et al. (2010). C/EBPbeta controls exercise-induced cardiac growth and protects against pathological cardiac remodeling. Cell *143*, 1072–1083.
15. Bezzerides, V.J., Platt, C., Lerchenmuller, C., Paruchuri, K., Oh, N.L., Xiao, C., Cao, Y., Mann, N., Spiegelman, B.M., and Rosenzweig, A. (2016). CITED4 induces physiologic hypertrophy and promotes functional recovery after ischemic injury. JCI Insight *1*, e85904.
16. Gao, R., Wang, L., Bei, Y., Wu, X., Wang, J., Zhou, Q., Tao, L., Das, S., Li, X., and Xiao, J. (2021). Long noncoding RNA cardiac physiological hypertrophy-associated regulator induces cardiac physiological hypertrophy and promotes functional recovery after myocardial ischemia-reperfusion injury. Circulation *144*, 303–317.
17. Shi, J., Bei, Y., Kong, X., Liu, X., Lei, Z., Xu, T., Wang, H., Xuan, Q., Chen, P., Xu, J., et al. (2017). miR-17-3p contributes to exercise-induced cardiac growth and protects against myocardial ischemia-reperfusion injury. Theranostics *7*, 664–676.
18. Liu, X., Xiao, J., Zhu, H., Wei, X., Platt, C., Damilano, F., Xiao, C., Bezzerides, V., Bostrom, P., Che, L., et al. (2015). miR-222 is necessary for exercise-induced cardiac growth and protects against pathological cardiac remodeling. Cell Metab. *21*, 584–595.
19. Lopez-Bertoni, H., Kotchetkov, I.S., Mihelson, N., Lal, B., Rui, Y., Ames, H., Lugo-Fagundo, M., Guerrero-Cazares, H., Quinones-Hinojosa, A., Green, J.J., et al. (2020). A sox2:miR-486-5p Axis regulates survival of GBM cells by inhibiting tumor suppressor networks. Cancer Res. *80*, 1644–1655.
20. Ola, R., Kunzel, S.H., Zhang, F., Genet, G., Chakraborty, R., Pibouin-Fragner, L., Martin, K., Sessa, W., Dubrac, A., and Eichmann, A. (2018). SMAD4 prevents flow induced arteriovenous malformations by inhibiting casein kinase 2. Circulation *138*, 2379–2394.

21. Zhao, H., Yang, H., Geng, C., Chen, Y., Tang, Y., Li, Z., Pang, J., Shu, T., Nie, Y., Liu, Y., et al. (2021). Elevated IgE promotes cardiac fibrosis by suppressing miR-486a-5p. Theranostics *11*, 7600–7615.

22. Hill, J.A. (2015). Braking bad hypertrophy. N. Engl. J. Med. *372*, 2160–2162.

23. Bei, Y., Pan, L.L., Zhou, Q., Zhao, C., Xie, Y., Wu, C., Meng, X., Gu, H., Xu, J., Zhou, L., et al. (2019). Cathelicidin-related antimicrobial peptide protects against myocardial ischemia/reperfusion injury. BMC Med. *17*, 42.

24. Sun, X.H., Wang, X., Zhang, Y., and Hui, J. (2019). Exosomes of bone-marrow stromal cells inhibit cardiomyocyte apoptosis under ischemic and hypoxic conditions via miR-486-5p targeting the PTEN/PI3K/AKT signaling pathway. Thromb. Res. *177*, 23–32.

25. Jae, N., and Dimmeler, S. (2020). Noncoding RNAs in vascular diseases. Circ. Res. *126*, 1127–1145.

26. Ruan, H., Li, J., Ren, S., Gao, J., Li, G., Kim, R., Wu, H., and Wang, Y. (2009). Inducible and cardiac specific PTEN inactivation protects ischemia/reperfusion injury. J. Mol. Cell Cardiol. *46*, 193–200.

27. Lange, S., Banerjee, I., Carrion, K., Serrano, R., Habich, L., Kameny, R., Lengenfelder, L., Dalton, N., Meili, R., Borgeson, E., et al. (2019). miR-486 is modulated by stretch and increases ventricular growth. JCI Insight *4*, e125507.

28. Wendel, H.G., De Stanchina, E., Fridman, J.S., Malina, A., Ray, S., Kogan, S., Cordon-Cardo, C., Pelletier, J., and Lowe, S.W. (2004). Survival signalling by Akt and eIF4E in oncogenesis and cancer therapy. Nature *428*, 332–337.

29. Yue, H.W., Liu, J., Liu, P.P., Li, W.J., Chang, F., Miao, J.Y., and Zhao, J. (2015). Sphingosylphosphorylcholine protects cardiomyocytes against ischemic apoptosis via lipid raft/PTEN/Akt1/mTOR mediated autophagy. Biochim. Biophys. Acta. *1851*, 1186–1193.

30. Lu, C., Wang, X., Ha, T., Hu, Y., Liu, L., Zhang, X., Yu, H., Miao, J., Kao, R., Kalbfleisch, J., et al. (2015). Attenuation of cardiac dysfunction and remodeling of myocardial infarction by microRNA-130a are mediated by suppression of PTEN and activation of PI3K dependent signaling. J. Mol. Cell Cardiol. *89*, 87–97.

31. Zhang, X., Tang, N., Hadden, T.J., and Rishi, A.K. (2011). Akt, FoxO and regulation of apoptosis. Biochim. Biophys. Acta. *1813*, 1978–1986.

32. Puthanveetil, P., Wan, A., and Rodrigues, B. (2013). FoxO1 is crucial for sustaining cardiomyocyte metabolism and cell survival. Cardiovasc. Res. *97*, 393–403.

33. Haase, A., Gohring, G., and Martin, U. (2017). Generation of non-transgenic iPS cells from human cord blood CD34(+) cells under animal component-free conditions. Stem Cell Res. *21*, 71–73.

34. Zangi, L., Oliveira, M.S., Ye, L.Y., Ma, Q., Sultana, N., Hadas, Y., Chepurko, E., Spater, D., Zhou, B., Chew, W.L., et al. (2017). Insulin-like growth factor 1 receptor-dependent pathway drives epicardial adipose tissue formation after myocardial injury. Circulation *135*, 59–72.

35. Tohyama, S., Hattori, F., Sano, M., Hishiki, T., Nagahata, Y., Matsuura, T., Hashimoto, H., Suzuki, T., Yamashita, H., Satoh, Y., et al. (2013). Distinct metabolic flow enables large-scale purification of mouse and human pluripotent stem cell-derived cardiomyocytes. Cell Stem Cell *12*, 127–137.

36. Foinquinos, A., Batkai, S., Genschel, C., Viereck, J., Rump, S., Gyongyosi, M., Traxler, D., Riesenhuber, M., Spannbauer, A., Lukovic, D., et al. (2020). Preclinical development of a miR-132 inhibitor for heart failure treatment. Nat. Commun. *11*, 633.

YMTHE, Volume *30*

Supplemental Information

miR-486 attenuates cardiac ischemia/reperfusion injury and mediates the beneficial effect of exercise for myocardial protection

Yihua Bei, Dongchao Lu, Christian Bär, Shambhabi Chatterjee, Alessia Costa, Isabelle Riedel, Frank C. Mooren, Yujiao Zhu, Zhenzhen Huang, Meng Wei, Meiyu Hu, Sunyi Liu, Pujiao Yu, Kun Wang, Thomas Thum, and Junjie Xiao

Supplemental Figures

Figure S1

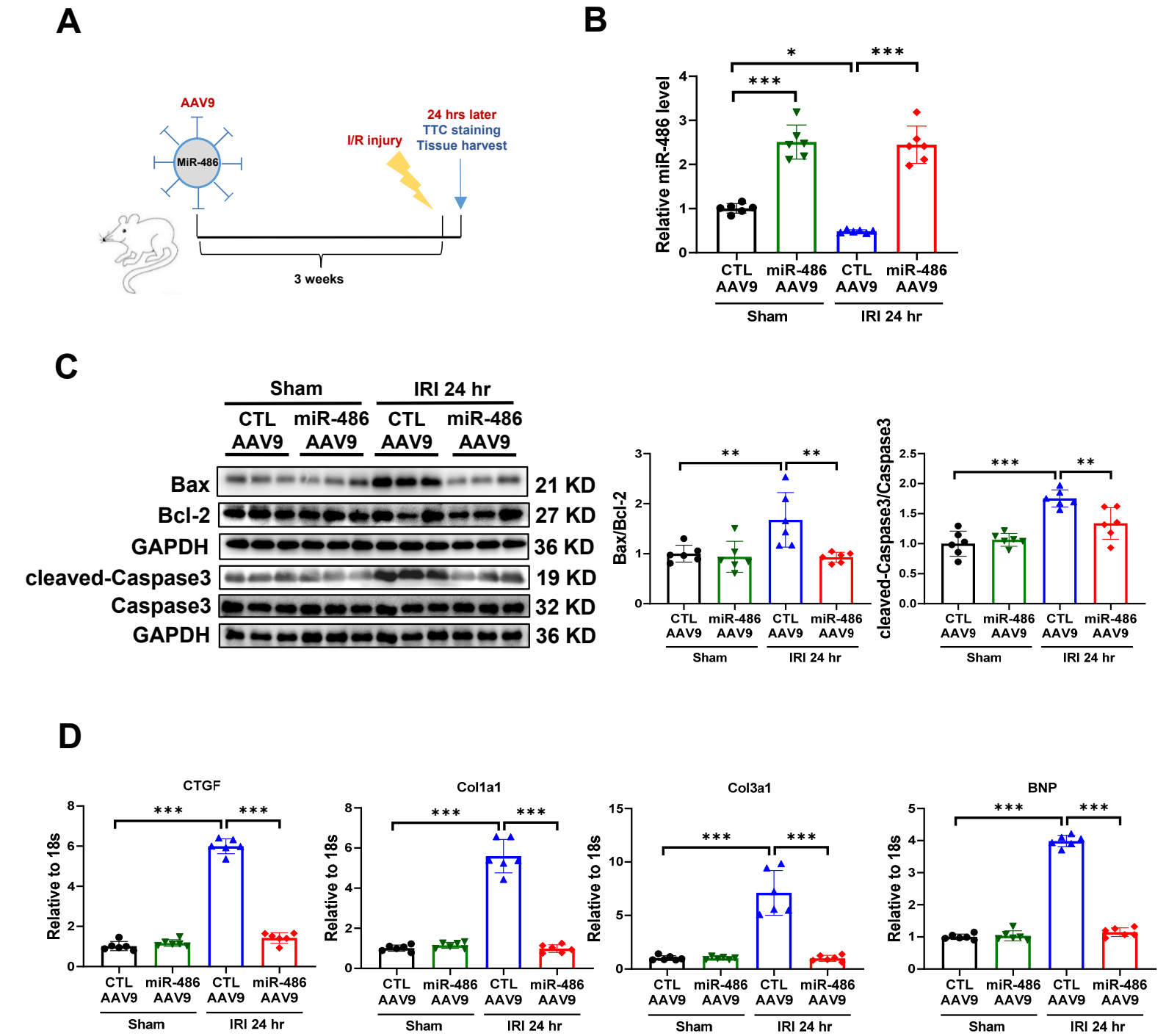
A
AAV9
MiR-486
I/R injury
24 hrs later
TTC staining
Tissue harvest
3 weeks
B
Relative miR-486 level
CTL AAV9
miR-486 AAV9
CTL AAV9
miR-486 AAV9
Sham
IRI 24 hr
C
Sham
IRI 24 hr
CTL AAV9
miR-486 AAV9
CTL AAV9
miR-486 AAV9
Bax
Bcl-2
GAPDH
cleaved-Caspase3
Caspase3
GAPDH
21 KD
27 KD
36 KD
19 KD
32 KD
36 KD
Bax/Bcl-2
cleaved-Caspase3/Caspase3
D
CTGF
Col1a1
Col3a1
BNP
Relative to 18s

Figure S2

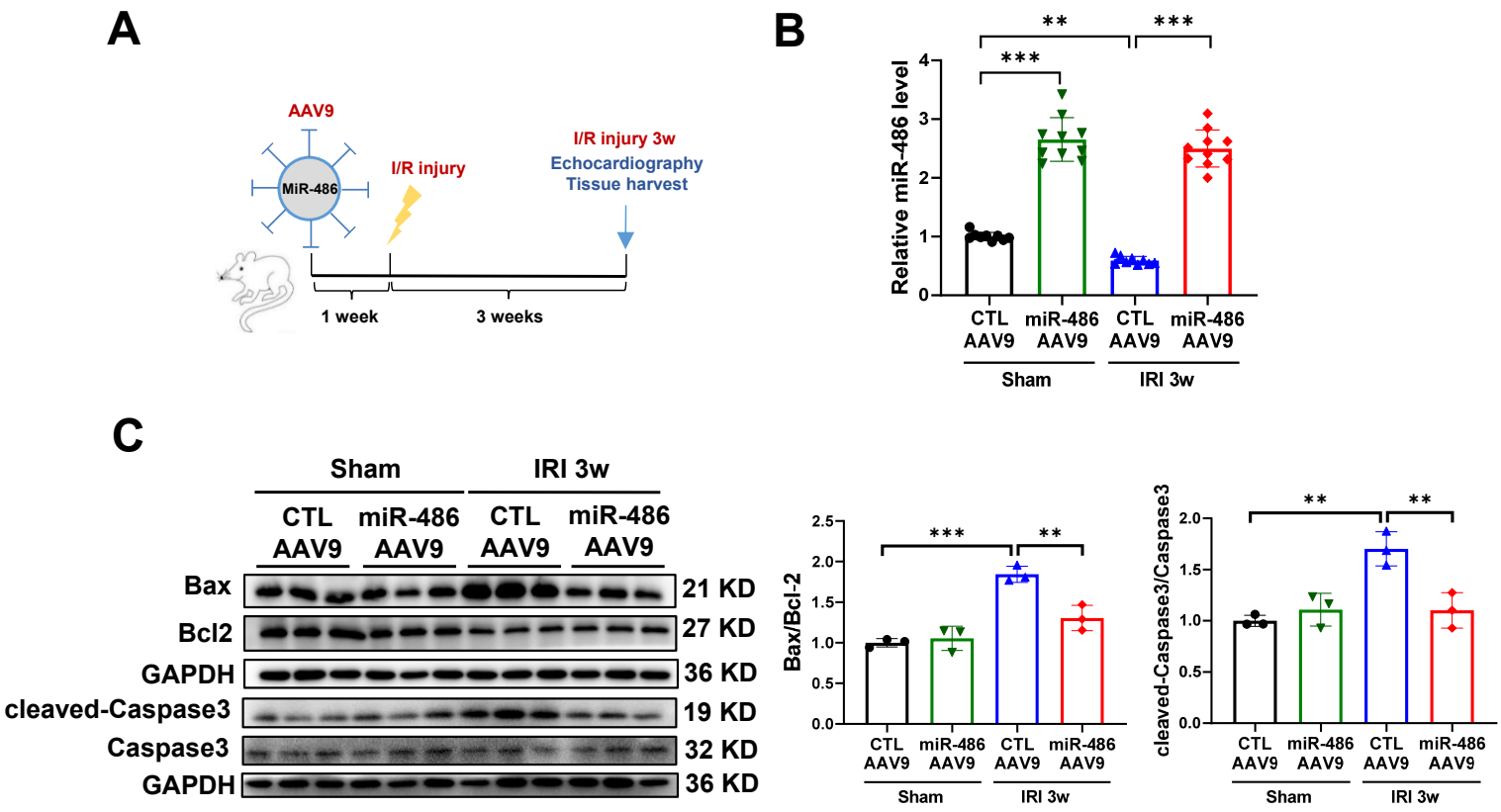
A
AAV9
MiR-486
I/R injury
I/R injury 3w
Echocardiography
Tissue harvest
1 week
3 weeks
B
Relative miR-486 level
CTL AAV9
miR-486 AAV9
Sham
IRI 3w
C
Sham
IRI 3w
Bax
Bcl2
GAPDH
cleaved-Caspase3
Caspase3
GAPDH
21 KD
27 KD
36 KD
19 KD
32 KD
36 KD
Bax/Bcl-2
cleaved-Caspase3/Caspase3

Figure S3

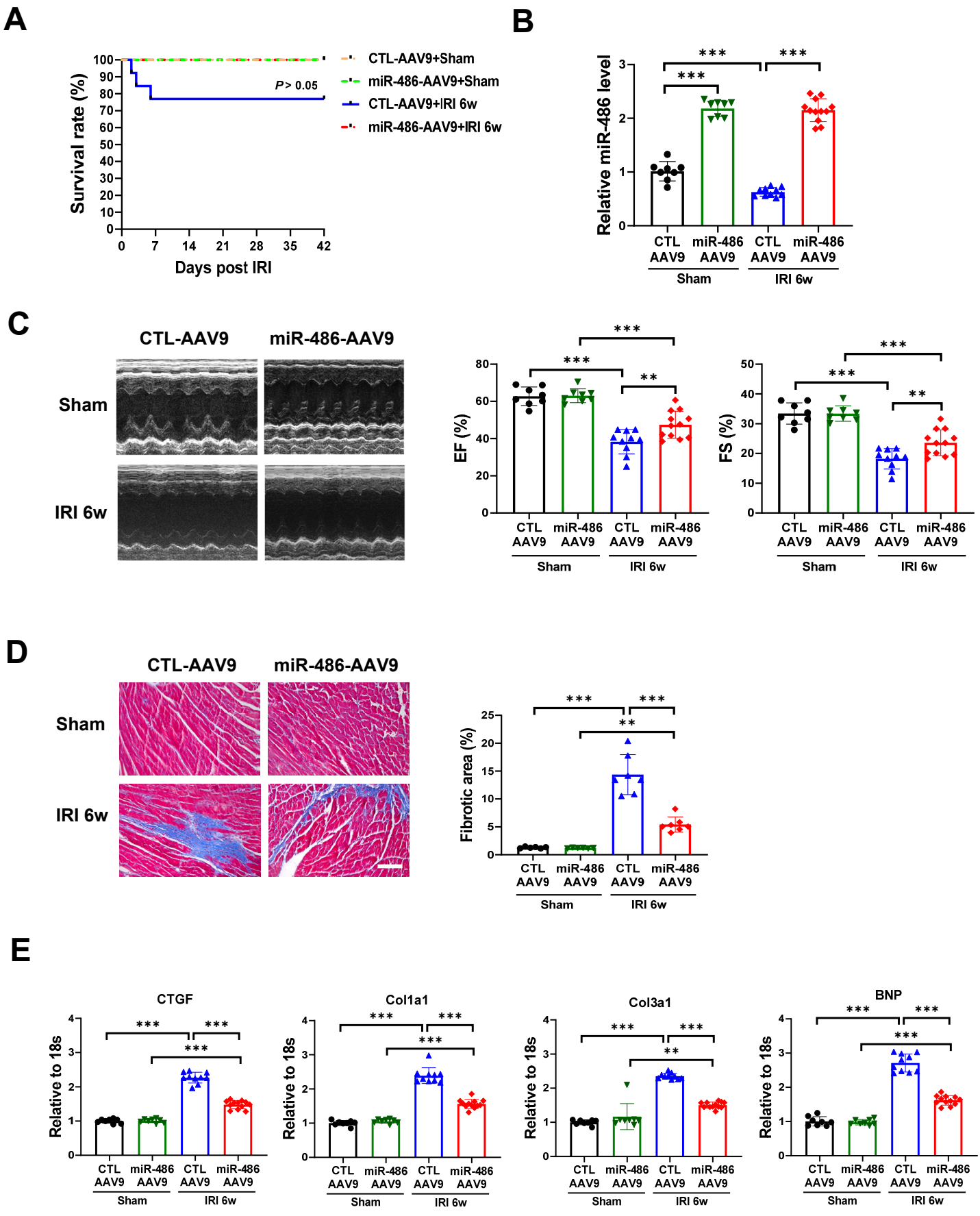
A
Survival rate (%)
Days post IRI
P> 0.05
CTL-AAV9+Sham
miR-486-AAV9+Sham
CTL-AAV9+IRI 6w
miR-486-AAV9+IRI 6w
B
Relative miR-486 level
CTL AAV9
miR-486 AAV9
Sham
IRI 6w
C
CTL-AAV9
miR-486-AAV9
Sham
IRI 6w
EF (%)
FS (%)
D
Fibrotic area (%)
E
CTGF
Col1a1
Col3a1
BNP
Relative to 18s

Figure S4

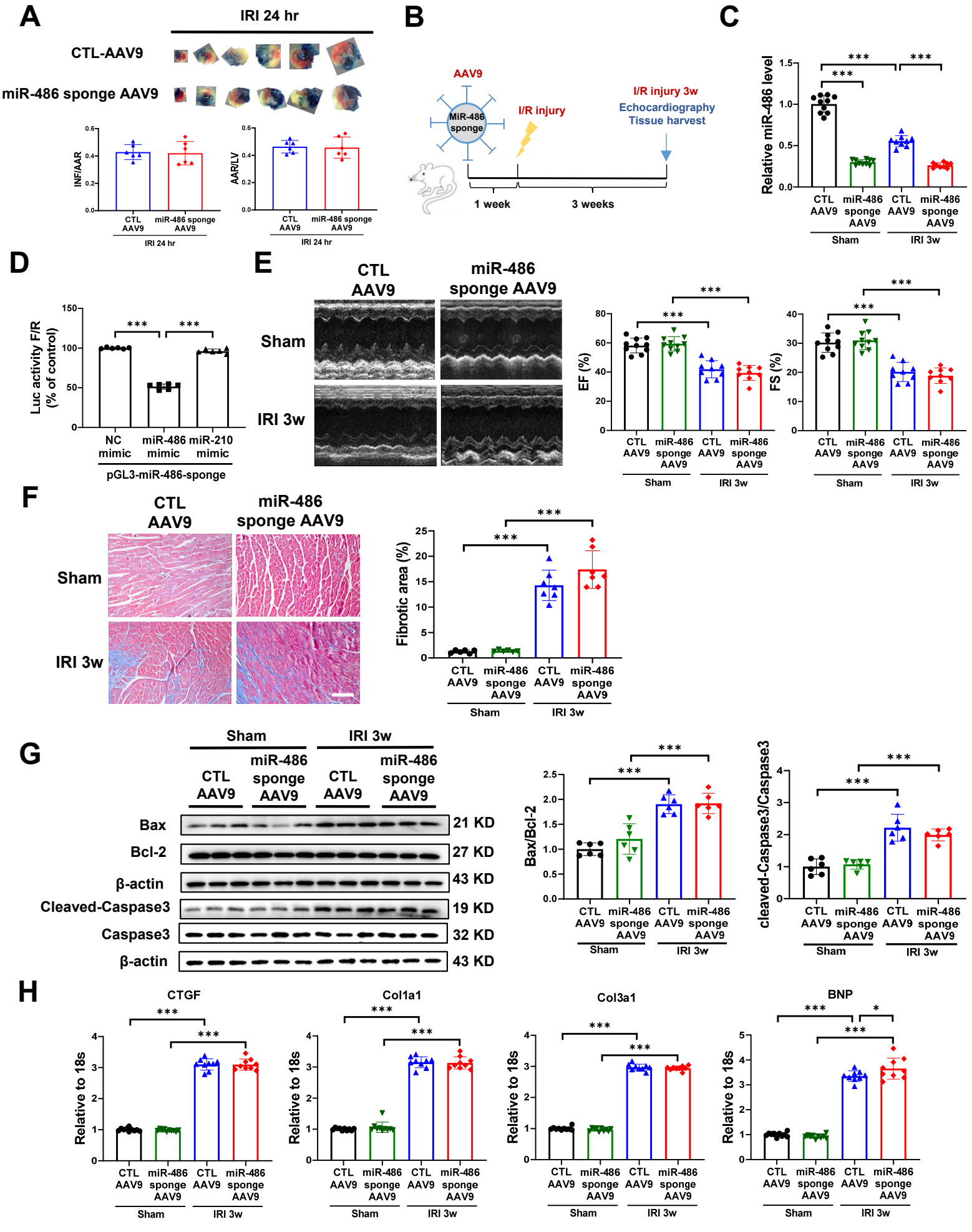
A
IRI 24 hr
CTL-AAV9
miR-486 sponge AAV9
INF/AAR
AAR/LV
CTL AAV9
miR-486 sponge AAV9
IRI 24 hr
B
AAV9
MiR-486 sponge
I/R injury
I/R injury 3w
Echocardiography
Tissue harvest
1 week
3 weeks
C
Relative miR-486 level
Sham
IRI 3w
D
Luc activity F/R (% of control)
NC mimic
miR-486 mimic
miR-210 mimic
pGL3-miR-486-sponge
E
CTL AAV9
miR-486 sponge AAV9
Sham
IRI 3w
EF (%)
FS (%)
F
Fibrotic area (%)
G
Bax
Bcl-2
β-actin
Cleaved-Caspase3
Caspase3
β-actin
21 KD
27 KD
43 KD
19 KD
32 KD
43 KD
Bax/Bcl-2
cleaved-Caspase3/Caspase3
H
CTGF
Col1a1
Col3a1
BNP
Relative to 18s

Figure S5

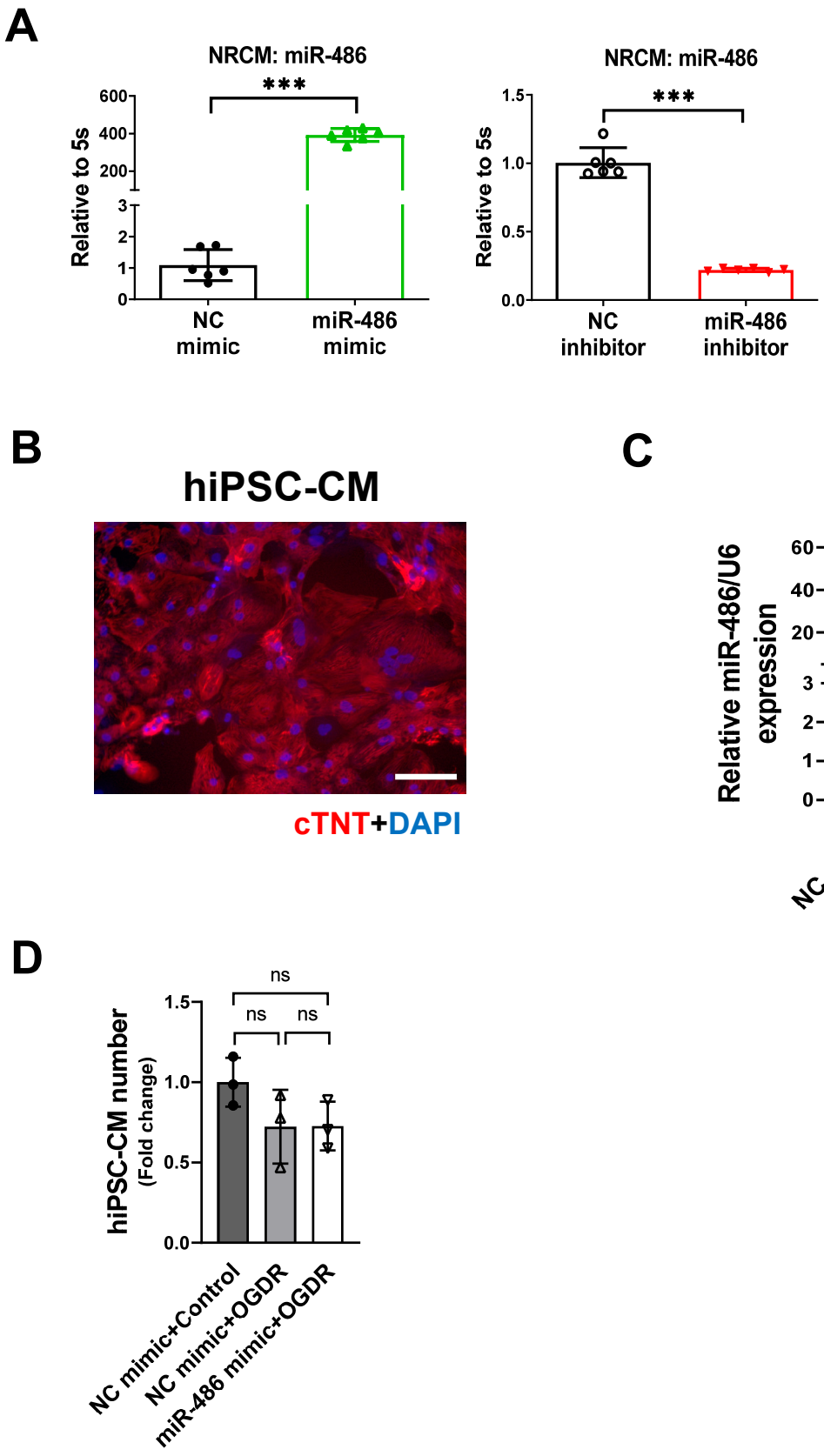
A
NRCM: miR-486
***
Relative to 5s
600
400
200
3
2
1
0
NC mimic
miR-486 mimic
NRCM: miR-486
***
Relative to 5s
1.5
1.0
0.5
0.0
NC inhibitor
miR-486 inhibitor
B
hiPSC-CM
cTNT+DAPI
C
hiPSC-CM
*
Relative miR-486/U6 expression
60
40
20
3
2
1
0
NC mimic
miR-486 mimic
D
ns
ns
ns
hiPSC-CM number
(Fold change)
1.5
1.0
0.5
0.0
NC mimic+Control
NC mimic+OGDR
miR-486 mimic+OGDR

Figure S6

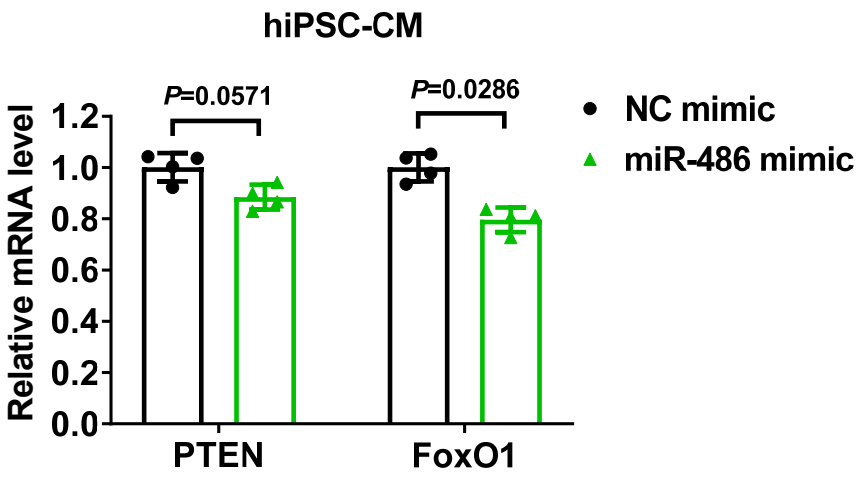
hiPSC-CM
P=0.0571
P=0.0286
Relative mRNA level
1.2
1.0
0.8
0.6
0.4
0.2
0.0
PTEN
FoxO1
NC mimic
miR-486 mimic

Figure S7

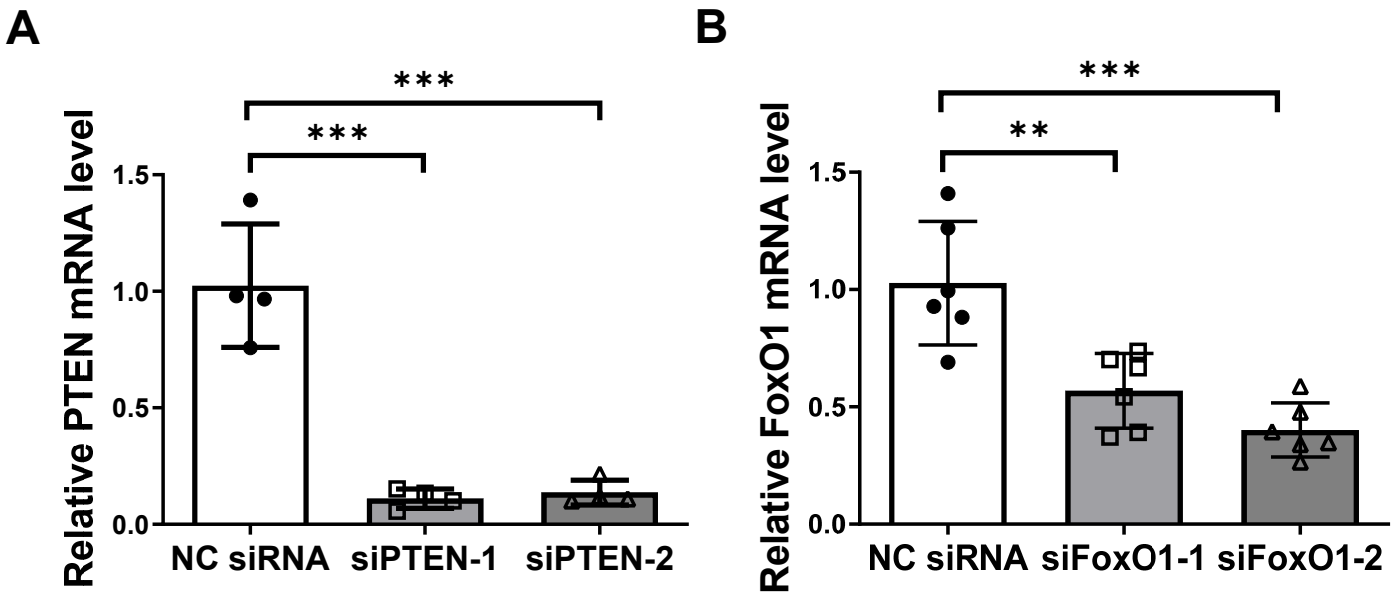
A
***
***
Relative PTEN mRNA level
1.5
1.0
0.5
0.0
NC siRNA
siPTEN-1
siPTEN-2
B
***
**
Relative FoxO1 mRNA level
1.5
1.0
0.5
0.0
NC siRNA
siFoxO1-1
siFoxO1-2

Figure S8

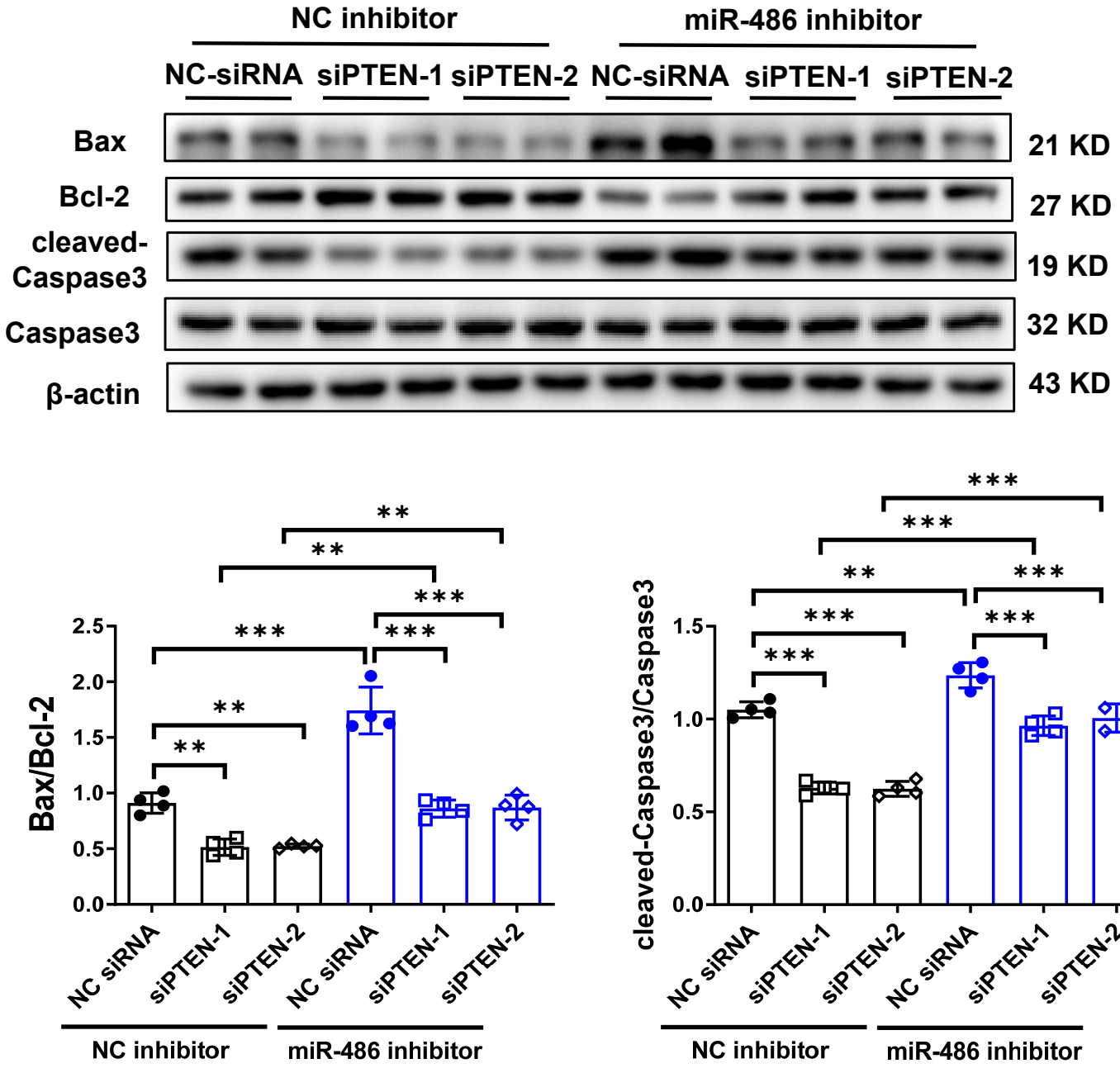
NC inhibitor
miR-486 inhibitor
NC-siRNA
siPTEN-1
siPTEN-2
NC-siRNA
siPTEN-1
siPTEN-2
Bax
Bcl-2
cleaved-Caspase3
Caspase3
β-actin
21 KD
27 KD
19 KD
32 KD
43 KD
Bax/Bcl-2
cleaved-Caspase3/Caspase3
NC siRNA
siPTEN-1
siPTEN-2
NC siRNA
siPTEN-1
siPTEN-2
NC inhibitor
miR-486 inhibitor

Figure S9

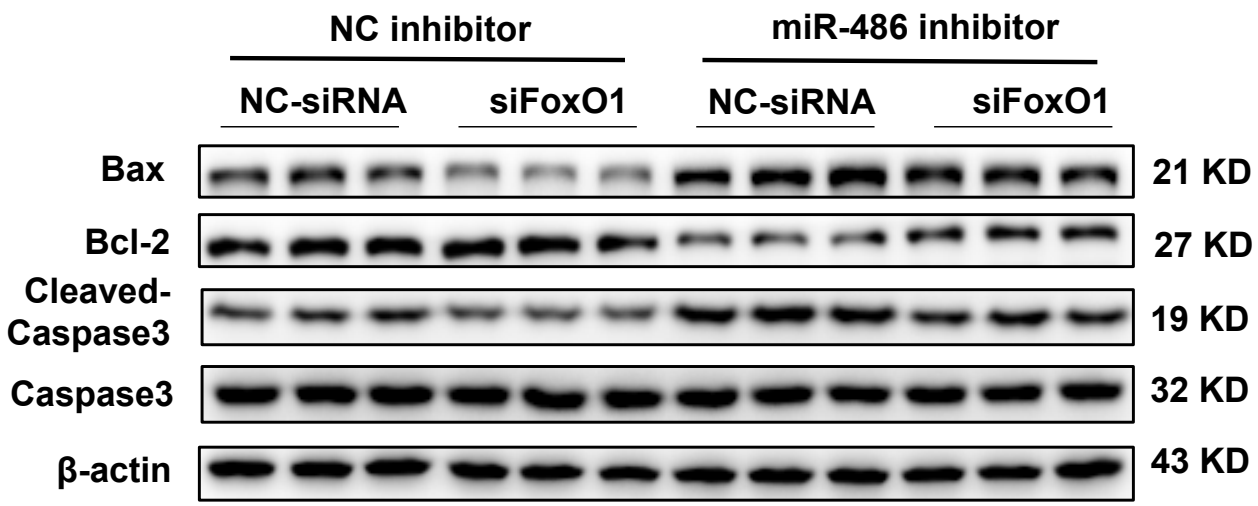
NC inhibitor
miR-486 inhibitor
NC-siRNA
siFoxO1
NC-siRNA
siFoxO1
Bax
Bcl-2
Cleaved-Caspase3
Caspase3
β-actin
21 KD
27 KD
19 KD
32 KD
43 KD

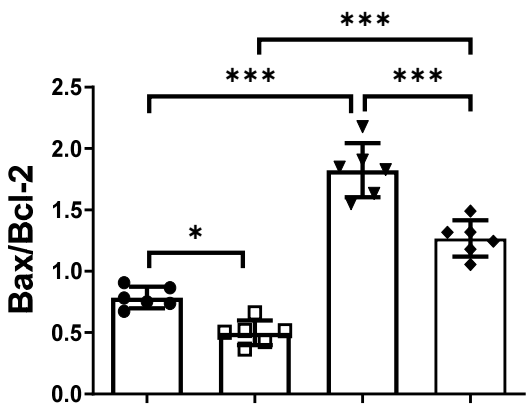
Bax/Bcl-2
2.5
2.0
1.5
1.0
0.5
0.0
***
***
***
*

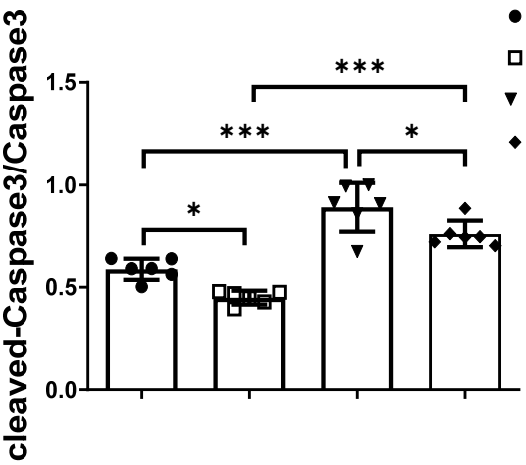
cleaved-Caspase3/Caspase3
1.5
1.0
0.5
0.0
***
***
*
*

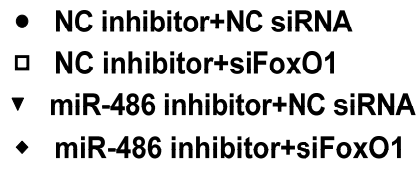
NC inhibitor+NC siRNA
NC inhibitor+siFoxO1
miR-486 inhibitor+NC siRNA
miR-486 inhibitor+siFoxO1

Figure S10

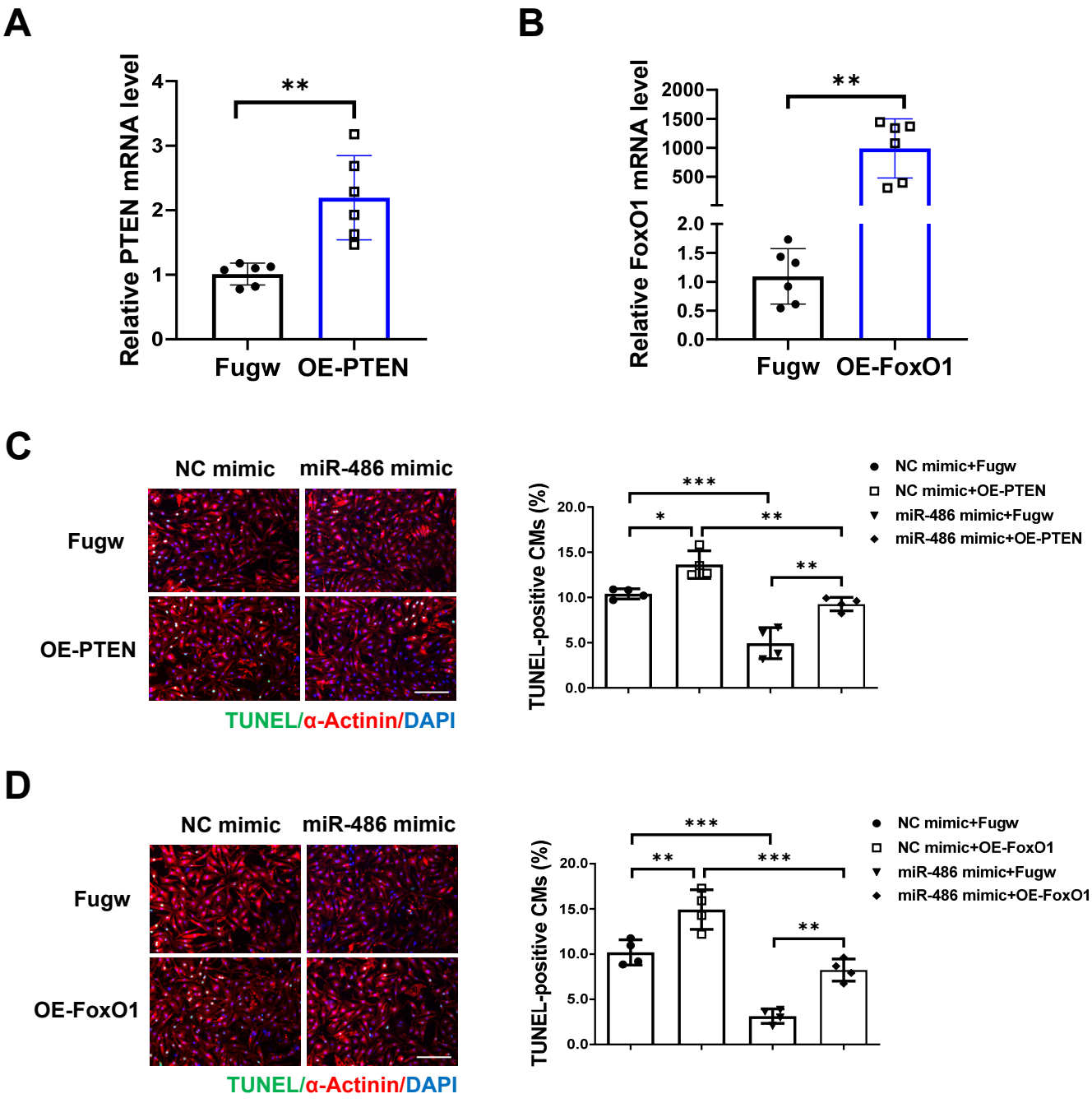
A
Relative PTEN mRNA level
**
Fugw
OE-PTEN
B
Relative FoxO1 mRNA level
**
Fugw
OE-FoxO1
C
NC mimic
miR-486 mimic
Fugw
OE-PTEN
TUNEL/α-Actinin/DAPI
TUNEL-positive CMs (%)
NC mimic+Fugw
NC mimic+OE-PTEN
miR-486 mimic+Fugw
miR-486 mimic+OE-PTEN
D
NC mimic
miR-486 mimic
Fugw
OE-FoxO1
TUNEL/α-Actinin/DAPI
TUNEL-positive CMs (%)
NC mimic+Fugw
NC mimic+OE-FoxO1
miR-486 mimic+Fugw
miR-486 mimic+OE-FoxO1

Figure S11

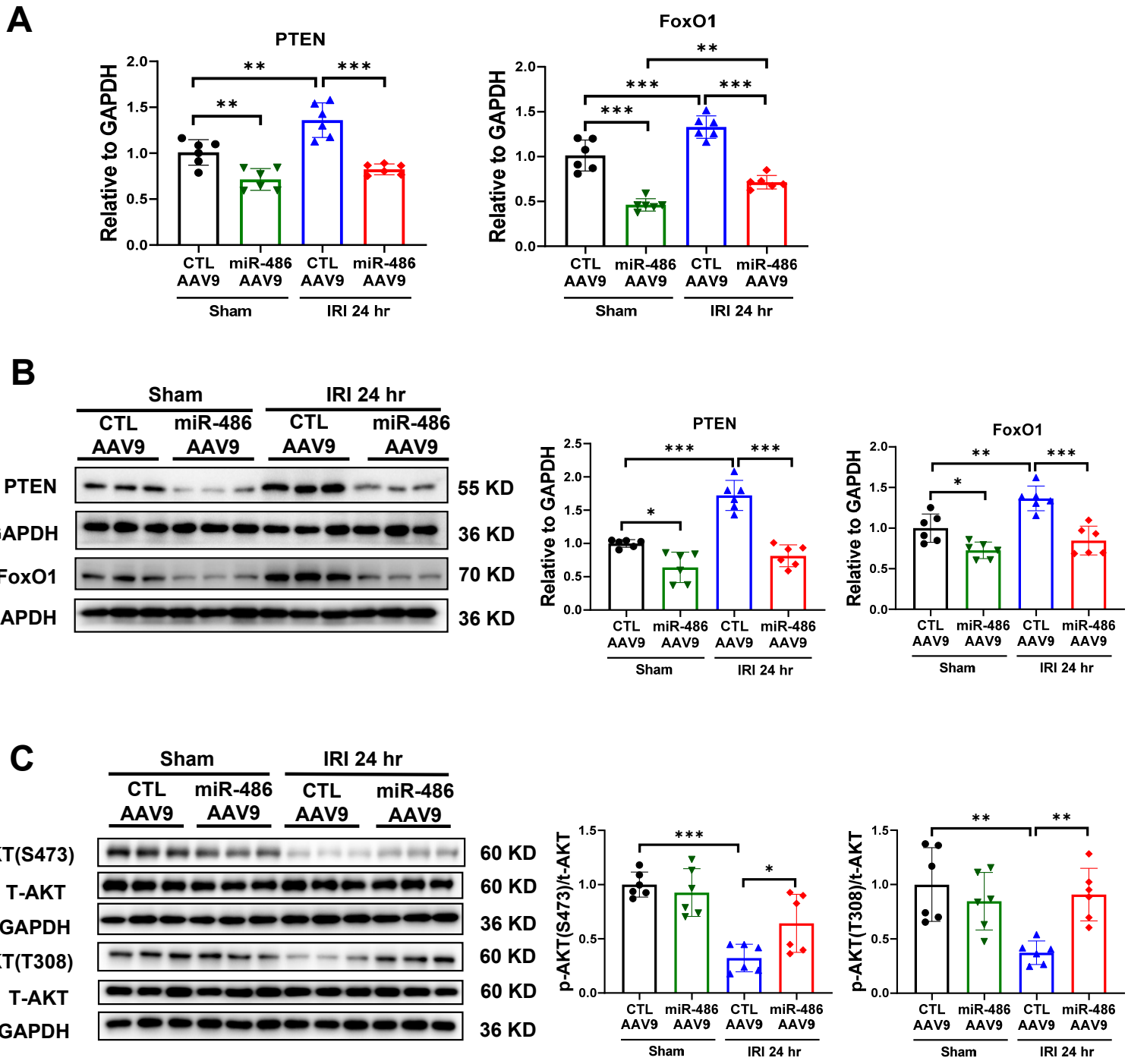
A
PTEN
Relative to GAPDH
2.0
1.5
1.0
0.5
0.0
**
**
***
CTL AAV9
miR-486 AAV9
CTL AAV9
miR-486 AAV9
Sham
IRI 24 hr
FoxO1
Relative to GAPDH
**
***
***
***
CTL AAV9
miR-486 AAV9
CTL AAV9
miR-486 AAV9
Sham
IRI 24 hr
B
Sham
IRI 24 hr
CTL AAV9
miR-486 AAV9
CTL AAV9
miR-486 AAV9
PTEN
GAPDH
FoxO1
GAPDH
55 KD
36 KD
70 KD
36 KD
PTEN
Relative to GAPDH
2.5
2.0
1.5
1.0
0.5
0.0
***
***
*
CTL AAV9
miR-486 AAV9
CTL AAV9
miR-486 AAV9
Sham
IRI 24 hr
FoxO1
Relative to GAPDH
2.0
1.5
1.0
0.5
0.0
**
***
*
CTL AAV9
miR-486 AAV9
CTL AAV9
miR-486 AAV9
Sham
IRI 24 hr
C
Sham
IRI 24 hr
CTL AAV9
miR-486 AAV9
CTL AAV9
miR-486 AAV9
p-AKT(S473)
T-AKT
GAPDH
p-AKT(T308)
T-AKT
GAPDH
60 KD
60 KD
36 KD
60 KD
60 KD
36 KD
p-AKT(S473)/t-AKT
1.5
1.0
0.5
0.0
***
*
CTL AAV9
miR-486 AAV9
CTL AAV9
miR-486 AAV9
Sham
IRI 24 hr
p-AKT(T308)/t-AKT
1.5
1.0
0.5
0.0
**
**
CTL AAV9
miR-486 AAV9
CTL AAV9
miR-486 AAV9
Sham
IRI 24 hr

Figure S12

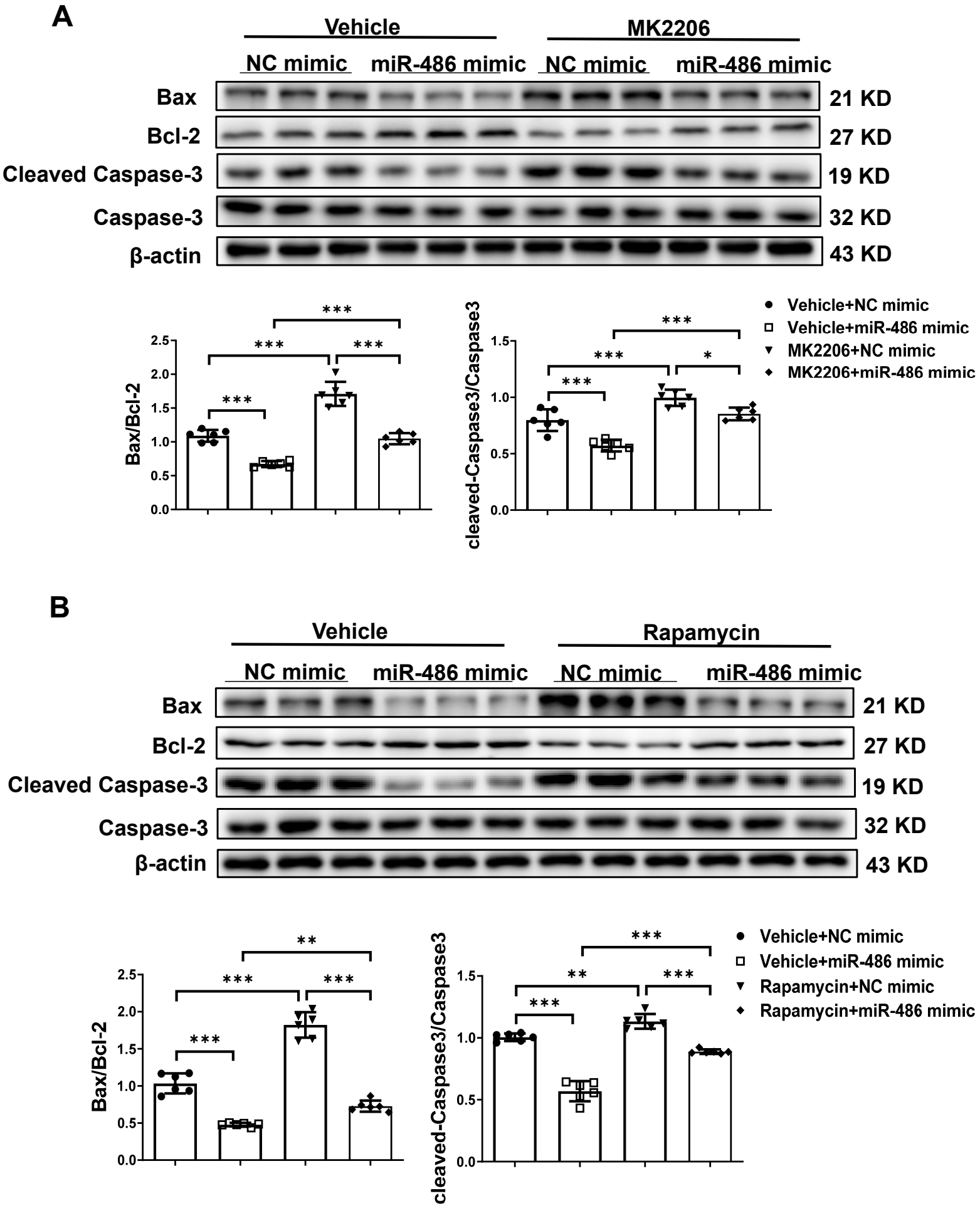
A
Vehicle
MK2206
NC mimic
miR-486 mimic
NC mimic
miR-486 mimic
Bax
Bcl-2
Cleaved Caspase-3
Caspase-3
β-actin
21 KD
27 KD
19 KD
32 KD
43 KD
Bax/Bcl-2
cleaved-Caspase3/Caspase3
Vehicle+NC mimic
Vehicle+miR-486 mimic
MK2206+NC mimic
MK2206+miR-486 mimic
B
Vehicle
Rapamycin
NC mimic
miR-486 mimic
NC mimic
miR-486 mimic
Bax
Bcl-2
Cleaved Caspase-3
Caspase-3
β-actin
21 KD
27 KD
19 KD
32 KD
43 KD
Bax/Bcl-2
cleaved-Caspase3/Caspase3
Vehicle+NC mimic
Vehicle+miR-486 mimic
Rapamycin+NC mimic
Rapamycin+miR-486 mimic

Figure S13

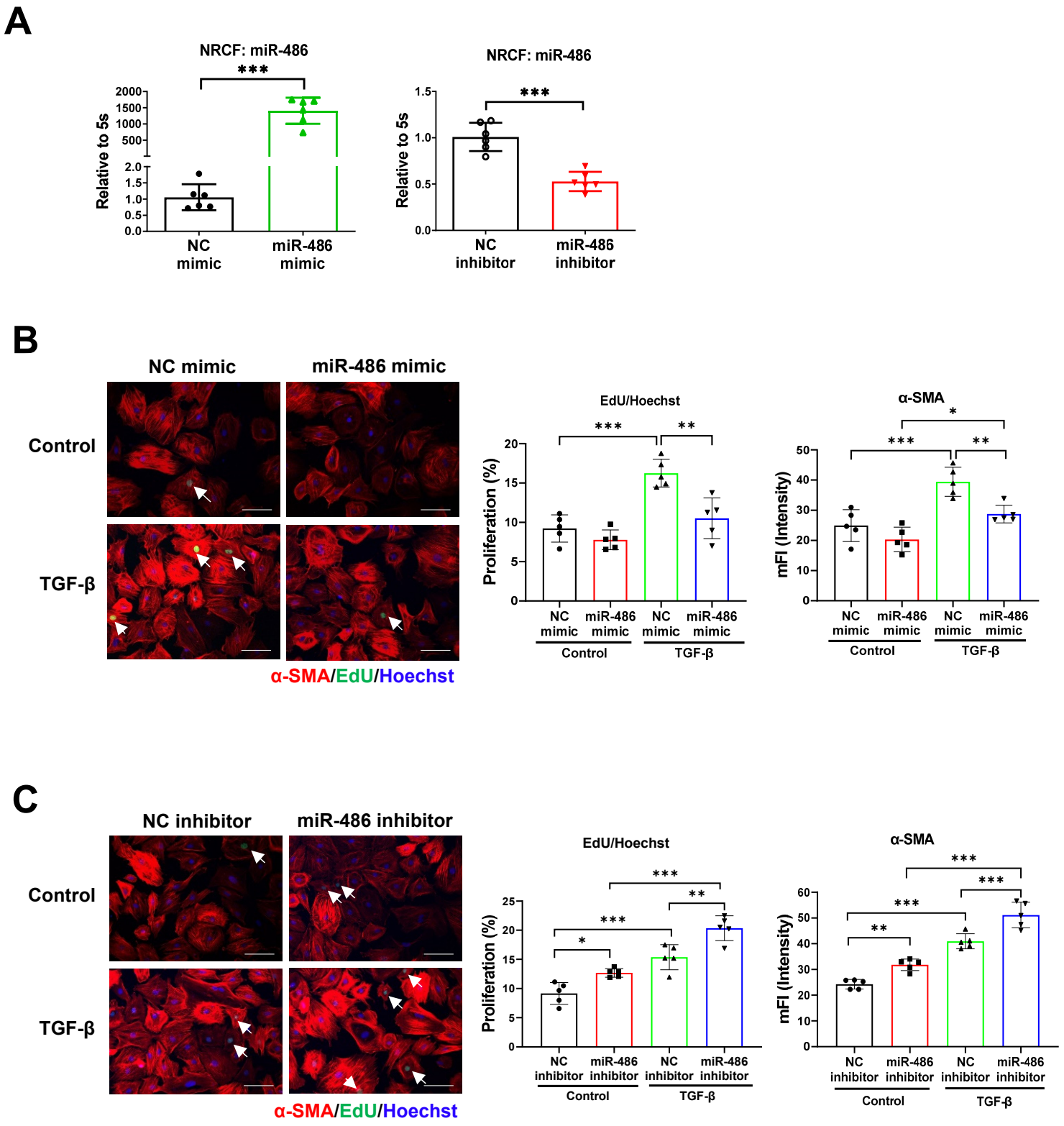
A
NRCF: miR-486
***
Relative to 5s
2000
1500
1000
500
2.0
1.5
1.0
0.5
0.0
NC mimic
miR-486 mimic
NRCF: miR-486
***
Relative to 5s
1.5
1.0
0.5
0.0
NC inhibitor
miR-486 inhibitor
B
NC mimic
miR-486 mimic
Control
TGF-β
α-SMA/EdU/Hoechst
EdU/Hoechst
***
**
Proliferation (%)
20
15
10
5
0
NC mimic
miR-486 mimic
NC mimic
miR-486 mimic
Control
TGF-β
α-SMA
*
***
**
mFI (Intensity)
50
40
30
20
10
0
NC mimic
miR-486 mimic
NC mimic
miR-486 mimic
Control
TGF-β
C
NC inhibitor
miR-486 inhibitor
Control
TGF-β
α-SMA/EdU/Hoechst
EdU/Hoechst
***
**
*
Proliferation (%)
25
20
15
10
5
0
NC inhibitor
miR-486 inhibitor
NC inhibitor
miR-486 inhibitor
Control
TGF-β
α-SMA
***
***
***
**
mFI (Intensity)
60
50
40
30
20
10
0
NC inhibitor
miR-486 inhibitor
NC inhibitor
miR-486 inhibitor
Control
TGF-β

Figure S14

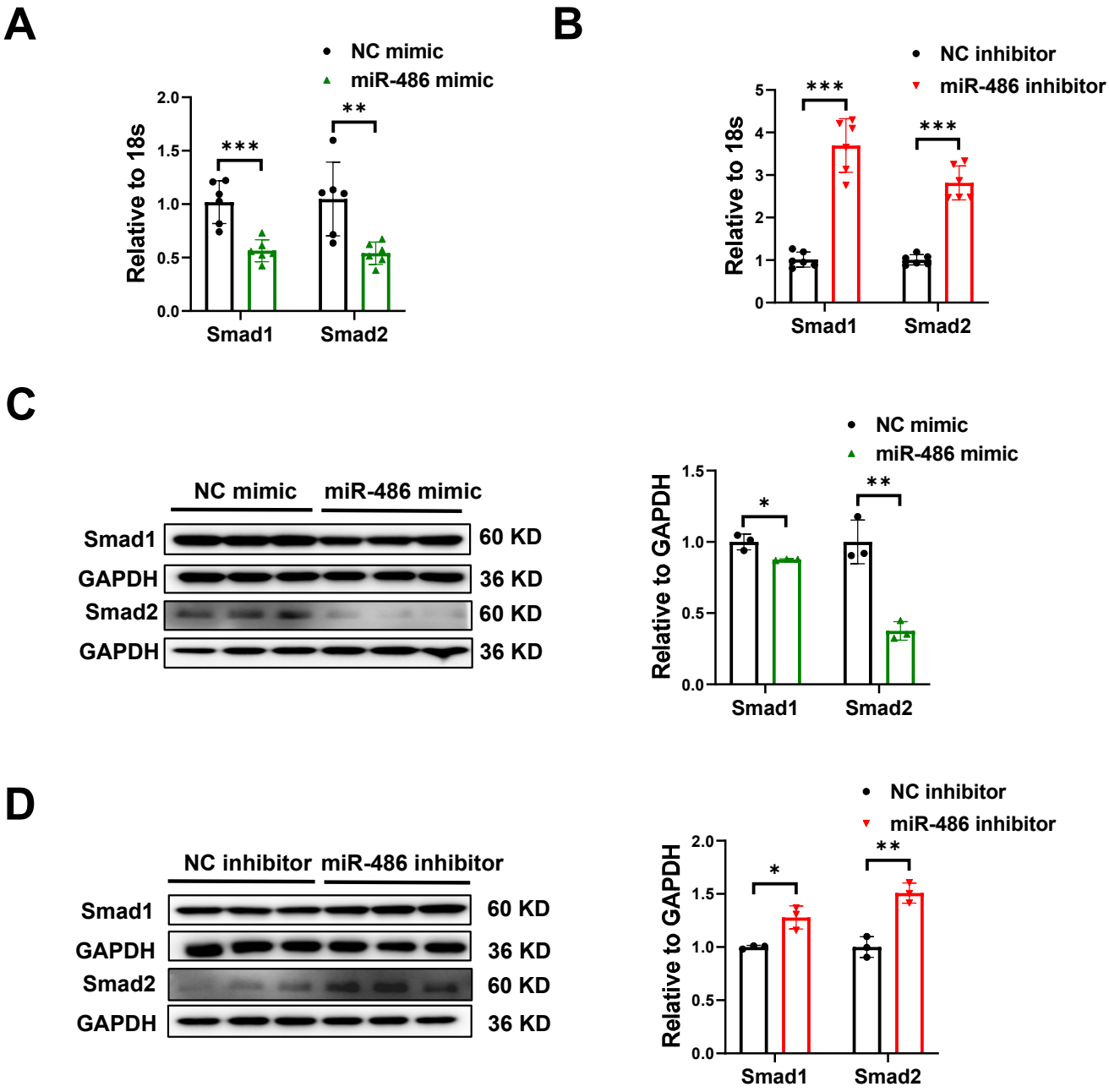
A
NC mimic
miR-486 mimic
Relative to 18s
2.0
1.5
1.0
0.5
0.0
***
**
Smad1
Smad2
B
NC inhibitor
miR-486 inhibitor
Relative to 18s
5
4
3
2
1
0
***
***
Smad1
Smad2
C
NC mimic
miR-486 mimic
Smad1
GAPDH
Smad2
GAPDH
60 KD
36 KD
60 KD
36 KD
NC mimic
miR-486 mimic
Relative to GAPDH
1.5
1.0
0.5
0.0
*
**
Smad1
Smad2
D
NC inhibitor
miR-486 inhibitor
Smad1
GAPDH
Smad2
GAPDH
60 KD
36 KD
60 KD
36 KD
NC inhibitor
miR-486 inhibitor
Relative to GAPDH
2.0
1.5
1.0
0.5
0.0
*
**
Smad1
Smad2

Figure S15

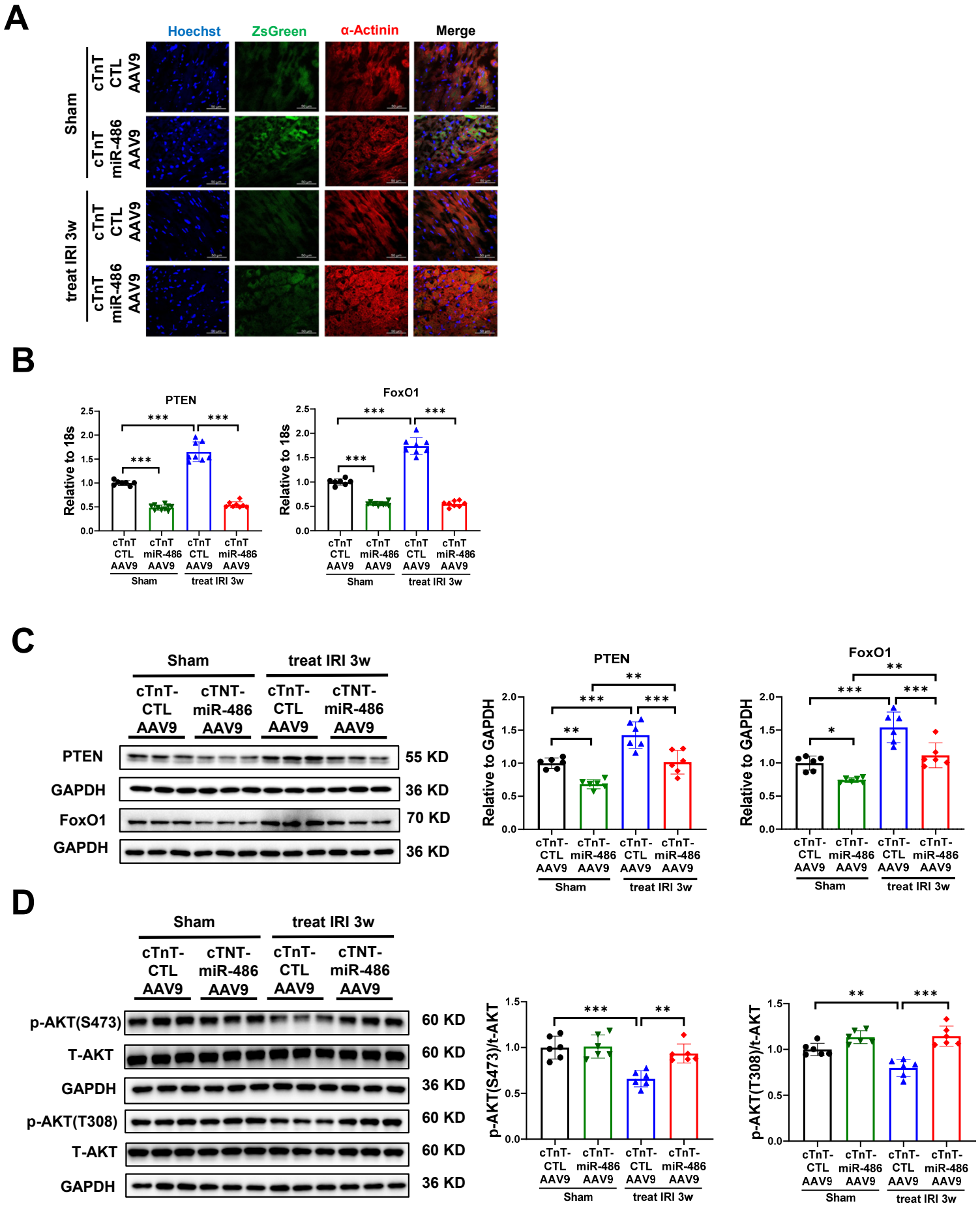
A
Hoechst
ZsGreen
α-Actinin
Merge
Sham
treat IRI 3w
cTnT CTL AAV9
cTnT miR-486 AAV9
B
PTEN
FoxO1
Relative to 18s
cTnT CTL AAV9
cTnT miR-486 AAV9
Sham
treat IRI 3w
C
Sham
treat IRI 3w
cTnT-CTL AAV9
cTNT-miR-486 AAV9
PTEN
GAPDH
FoxO1
55 KD
36 KD
70 KD
Relative to GAPDH
D
p-AKT(S473)
T-AKT
p-AKT(T308)
60 KD
p-AKT(S473)/t-AKT
p-AKT(T308)/t-AKT

Figure S16

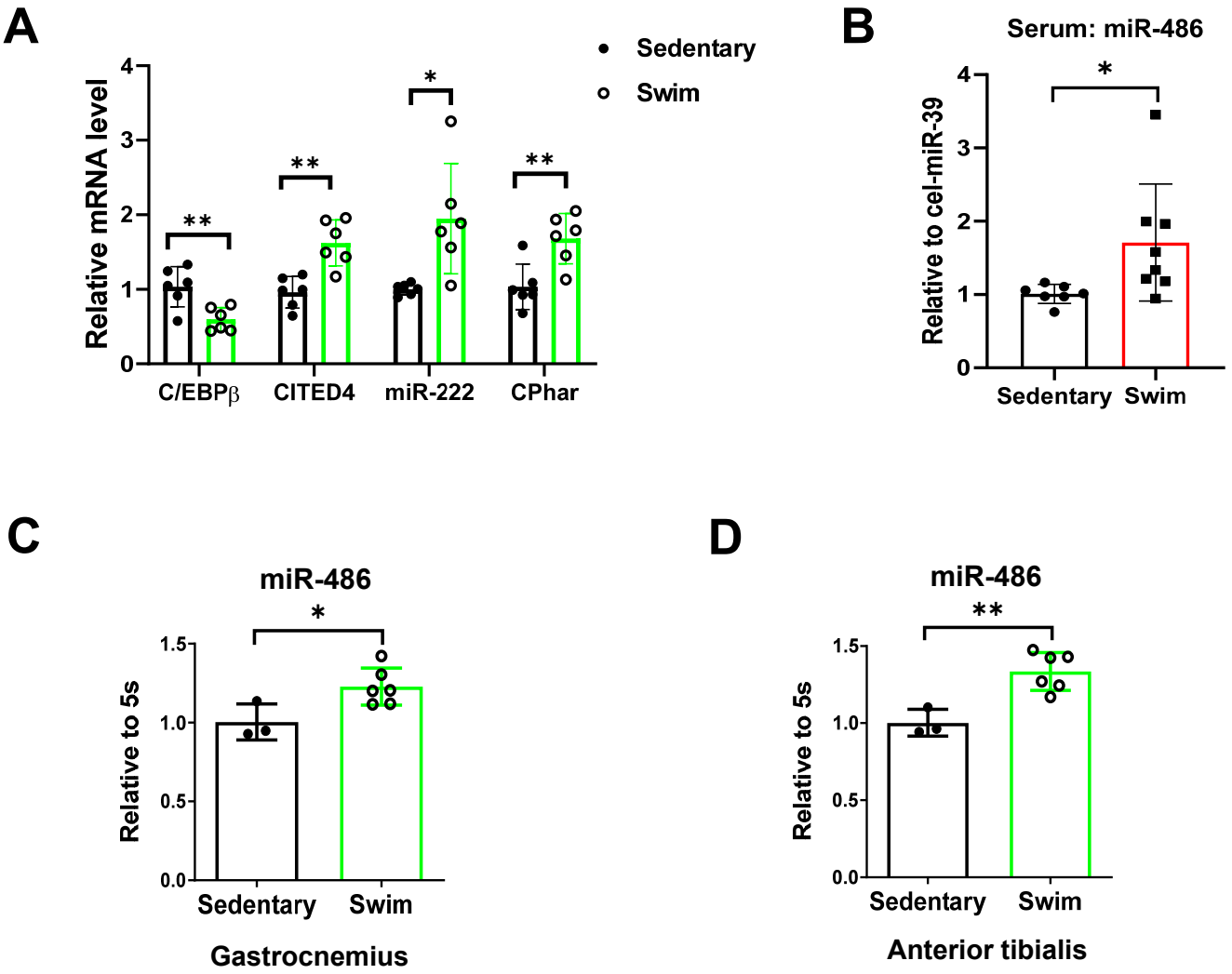
A
Sedentary
Swim
Relative mRNA level
C/EBPβ
CITED4
miR-222
CPhar
B
Serum: miR-486
Relative to cel-miR-39
Sedentary
Swim
C
miR-486
Relative to 5s
Sedentary
Swim
Gastrocnemius
D
miR-486
Relative to 5s
Sedentary
Swim
Anterior tibialis

Figure S17

A

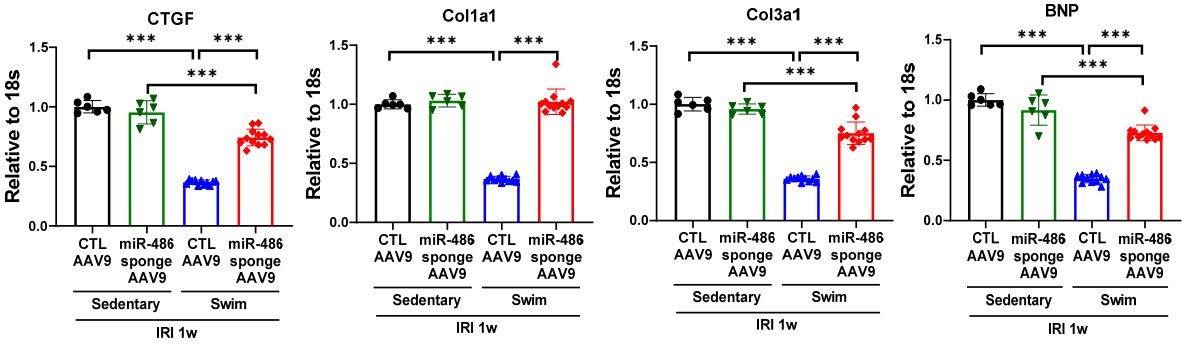

B

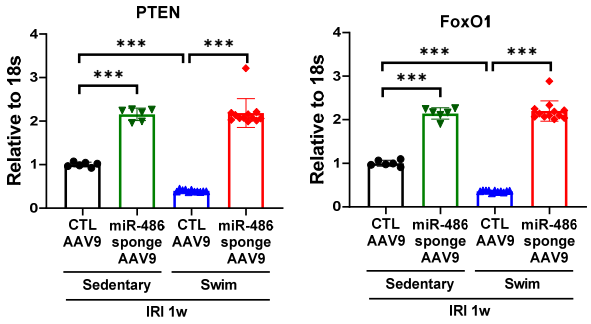

Figure S18

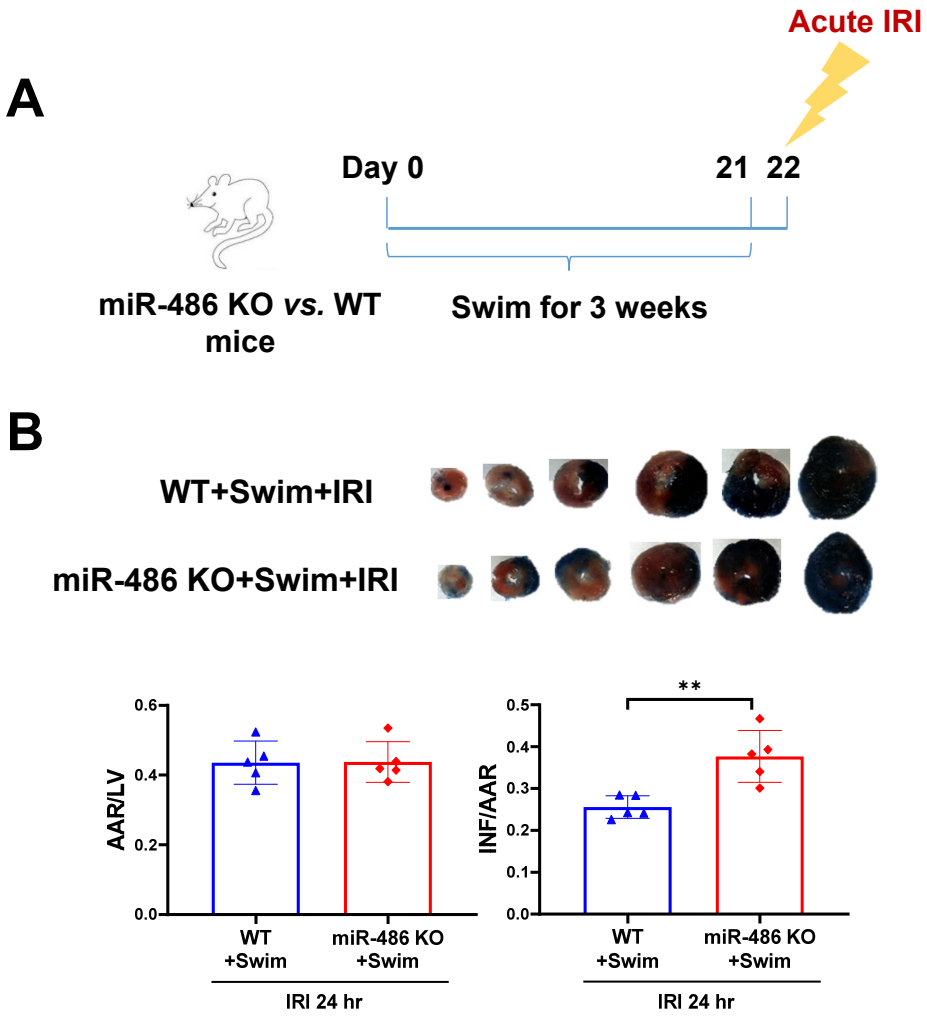
A
Acute IRI
Day 0
21 22
miR-486 KO vs. WT mice
Swim for 3 weeks
B
WT+Swim+IRI
miR-486 KO+Swim+IRI
AAR/LV
0.6
0.4
0.2
0.0
WT +Swim
miR-486 KO +Swim
IRI 24 hr
INF/AAR
0.5
0.4
0.3
0.2
0.1
0.0
**
WT +Swim
miR-486 KO +Swim
IRI 24 hr

Supplemental Figure Legends

Figure S1. Preventive intervention by miR-486-AAV9 in acute cardiac ischemia/reperfusion injury. (A) Schematic diagram showing that AAV9 expressing miR-486 (miR-486-AAV9) or AAV9 controls (CTL-AAV9) were injected via tail vein, and 3 weeks later mice were subjected to cardiac ischemia/reperfusion (I/R) injury for 24 hrs. (B) RT-PCR for miR-486 expression in mice heart tissues at 24 hrs post cardiac I/R injury (n=6). (C) Western blot for Bax/Bcl-2 ratio and cleaved-Caspase3/Caspase3 ratio in mice heart tissues (n=6). (D) RT-PCR for CTGF, Col1a1, Col3a1, and BNP expressions in mice heart tissues (n=6). Data were compared by two-way ANOVA test followed by Tukey post hoc test. *, $P<0.05$; **, $P<0.01$; ***, $P<0.001$.

Figure S2. Preventive intervention by miR-486-AAV9 in chronic cardiac ischemia/reperfusion injury. (A) Schematic diagram showing that AAV9 expressing miR-486 (miR-486-AAV9) or AAV9 controls (CTL-AAV9) were injected via tail vein, and 1 week later mice were subjected to cardiac ischemia/reperfusion (I/R) injury for 3 weeks. (B) RT-PCR for miR-486 expression in mice heart tissues at 3 weeks post cardiac I/R injury (n=9-10). (C) Western blot for Bax/Bcl-2 ratio and cleaved-Caspase3/Caspase3 ratio in mice heart tissues (n=3). Data were compared by two-way ANOVA test followed by Tukey post hoc test. **, $P<0.01$; ***, $P<0.001$.

Figure S3. Long term protective effect of miR-486 overexpression against cardiac ischemia/reperfusion injury and cardiac dysfunction over 6 weeks. (A) Survival rate of mice injected with miR-486-AAV9 or CTL-AAV9 after 6 weeks of cardiac ischemia/reperfusion (I/R) injury (n=8,8,13,12 before I/R injury, n=8,8,10,12 at 6 weeks post I/R injury). (B) RT-PCR for miR-486 expression in mice heart tissues at 6 weeks post cardiac I/R injury (n=8-12). (C) Echocardiography for left ventricular

ejection fraction (EF, %) and fractional shortening (FS, %) in mice at 6 week after I/R injury (n=8-12). (D) Masson Trichrome staining for cardiac fibrosis in mice heart tissues (n=6-7). Scale bar=100 μm. (E) RT-PCR for CTGF, Col1a1, Col3a1, and BNP expressions in mice heart tissues (n=8-12). Data were compared by two-way ANOVA test followed by Tukey post hoc test. **, $P<0.01$; ***, $P<0.001$.

Figure S4. Inhibition of miR-486 does not further aggravate cardiac ischemia/reperfusion injury. (A) The 2,3,5-triphenyltetrazolium chloride (TTC) staining for the infarct size at 24 hrs after cardiac ischemia/reperfusion (I/R) injury as determined by the infarct size/area at risk (INF/AAR) ratio. The area at risk/left ventricle weight (AAR/LV) ratio represents the homogeneity of surgery (n=6). (B) Schematic diagram showing that miR-486 sponge AAV9 or control AAV9 (CTL-AAV9) were injected via tail vein, and 1 week later mice were subjected to cardiac I/R injury for 3 weeks. (C) RT-PCR for miR-486 expression in mice heart tissues at 3 weeks post cardiac I/R injury (n=9-10). (D) Luciferase reporter assays performed in 293T cells co-transfected with negative control (NC mimic), miR-486 mimic or miR-210 mimic and the miR-486 binding site-carrying luciferase reporter plasmids (n=6). (E) Echocardiography for left ventricular ejection fraction (EF, %) and fractional shortening (FS, %) in mice at 3 week after I/R injury (n=9-10). (F) Masson Trichrome staining for cardiac fibrosis in mice heart tissues (n=6-7). Scale bar=100 μm. (G) Western blot for Bax/Bcl-2 ratio and cleaved-Caspase3/Caspase3 ratio in mice heart tissues (n=6). (H) RT-PCR for CTGF, Col1a1, Col3a1, and BNP expressions in mice heart tissues (n=9-10). Data between 2 groups were compared by unpaired two-tailed Student's t-test. Data among 3 groups were compared by one-way ANOVA test. Data among 4 groups were compared by two-way ANOVA test followed by Tukey post hoc test. *, $P<0.05$; ***, $P<0.001$.

Figure S5. Transfection of miR-486 mimic or inhibitor in cardiomyocytes *in vitro*. (A) RT-PCR for miR-486 expression in neonatal rat cardiomyocytes (NRCMs) transfected with miR-486 mimic, inhibitor, or negative controls (NC) (n=6). (B) Representative image of immunofluorescent staining for cardiac Troponin T (cTnT) which ensures the purification of human induced pluripotent stem cell-derived cardiomyocytes (hiPSC-CMs). Scale bar=100 μm. (C) RT-PCR for miR-486 expression in hiPSC-CMs transfected with miR-486 mimic or negative control (n=4). (D) Relative hiPSC-CM numbers after oxygen glucose deprivation/reperfusion (OGDR) and transfection of miR-486 mimic (n=3). Data between 2 groups were compared by unpaired two-tailed Student's t-test. Data among 3 groups were compared by one-way ANOVA test. *, $P<0.05$; ***, $P<0.001$.

Figure S6. Regulation of PTEN and FoxO1 in human induced pluripotent stem cell-derived cardiomyocytes with miR-486 overexpression. RT-PCR for PTEN and FoxO1 in human induced pluripotent stem cell-derived cardiomyocytes (hiPSC-CMs) transfected with miR-486 mimic or negative control (NC mimic) (n=4). Data were compared by unpaired two-tailed Student's t-test.

Figure S7. Si-RNAs significantly downregulate PTEN or FoxO1 expression in neonatal rat cardiomyocytes. (A,B) RT-PCR for PTEN (A) or FoxO1 (B) expressions in neonatal rat cardiomyocytes (NRCMs) transfected with siRNAs targeting PTEN or FoxO1, respectively (n=4-6). Data were compared between PTEN or FoxO1 siRNA group and NC siRNA group using unpaired two-tailed Student's t-test. **, $P<0.01$; ***, $P<0.001$.

Figure S8. Western blot for Bax/Bcl-2 ratio and cleaved-Caspase3/Caspase3 ratio in oxygen glucose deprivation/reperfusion-treated neonatal rat cardiomyocytes transfected with miR-486 inhibitor and PTEN siRNA. (n=4). Data were compared

by two-way ANOVA test followed by Tukey post hoc test. **, $P<0.01$; ***, $P<0.001$.

Figure S9. Western blot for Bax/Bcl-2 ratio and cleaved-Caspase3/Caspase3 ratio in oxygen glucose deprivation/reperfusion-treated neonatal rat cardiomyocytes transfected with miR-486 inhibitor and FoxO1 siRNA. (n=6). Data were compared by two-way ANOVA test followed by Tukey post hoc test. *, $P<0.05$; ***, $P<0.001$.

Figure S10. Overexpression of PTEN or FoxO1 attenuates the protective effect of miR-486 mimic against cardiomyocytes apoptosis. (A,B) RT-PCR for PTEN and FoxO1 in neonatal rat cardiomyocytes (NRCMs) transfected with plasmids expressing PTEN (A) or FoxO1 (B) (n=6). (C,D) TUNEL staining for α-Actinin-labelled NRCMs transfected with miR-486 mimic and plasmids expressing PTEN (C) or FoxO1 (D) in the condition of oxygen glucose deprivation/reperfusion (OGDR) treatment (n=4). Scale bar=100 μm. Data between 2 groups were compared by unpaired two-tailed Student's t-test. Data among 4 groups were compared by two-way ANOVA test followed by Tukey post hoc test. *, $P<0.05$; **, $P<0.01$; ***, $P<0.001$.

Figure S11. Preventive delivery of miR-486-AAV9 regulates PTEN and FoxO1 in mice heart tissues. (A,B) RT-PCR (A) and Western blot (B) for PTEN and FoxO1 expressions in heart tissues from mice injected with miR-486-AAV9 before cardiac ischemia/reperfusion (I/R) injury. Heart tissues were harvested at 24 hrs post I/R injury (n=6). (C) Western blot for AKT phosphorylation levels in heart tissues from mice injected with miR-486-AAV9 before cardiac I/R injury. Heart tissues were harvested at 24 hrs post I/R injury (n=6). Data were compared by two-way ANOVA test followed by Tukey post hoc test. *, $P<0.05$; **, $P<0.01$; ***, $P<0.001$.

Figure S12. MiR-486 inhibits cardiomyocyte apoptosis through activating AKT and mTOR. (A,B) Western blot for Bax/Bcl-2 ratio and cleaved-Caspase3/Caspase3 ratio in oxygen glucose deprivation/reperfusion (OGDR)-treated neonatal rat

cardiomyocytes transfected with miR-486 mimic in the presence or absence of AKT inhibitor MK2206 (A) or mTOR inhibitor Rapamycin (B) (n=6). Data were compared by two-way ANOVA test followed by Tukey post hoc test. *, $P<0.05$; **, $P<0.01$; ***, $P<0.001$.

Figure S13. MiR-486 inhibits cardiac fibroblast proliferation and activation. (A) RT-PCR for miR-486 in neonatal rat cardiac fibroblasts (NRCFs) transfected with miR-486 mimic, inhibitor, or negative controls (NC) (n=6). (B,C) Immunofluorescent staining for α-SMA/EdU in NRCFs transfected with miR-486 mimic (B), inhibitor (C), or NC (n=5). Scale bar=100 μm. Data between 2 groups were compared by unpaired two-tailed Student's t-test. Data among 4 groups were compared by two-way ANOVA test followed by Tukey post hoc test. *, $P<0.05$; **, $P<0.01$; ***, $P<0.001$.

Figure S14. MiR-486 negatively regulates Smad1 and Smad2 in cardiac fibroblasts. (A,B) RT-PCR for Smad1 and Smad2 in neonatal rat cardiac fibroblasts (NRCFs) transfected with miR-486 mimic (A), inhibitor (B), or negative controls (NC) (n=6). (C,D) Western blot for Smad1 and Smad2 in NRCFs transfected with miR-486 mimic (C), inhibitor (D), or NC (n=3). Data were compared by unpaired two-tailed Student's t-test. *, $P<0.05$; **, $P<0.01$; ***, $P<0.001$.

Figure S15. Therapeutic delivery of cTnT-miR-486 AAV9 regulates PTEN and FoxO1 in mice heart tissues. (A) Immunofluorescent imaging for co-localization of ZsGreen (indicative of AAV9) and α-Actinin staining in heart tissues from mice injected with cTnT-miR-486 AAV9 or cTnT-control AAV9. Scale bar=50 μm. (B,C) RT-PCR (B, n=7-10) and Western blot (C, n=6) for PTEN and FoxO1 expressions in heart tissues from mice treated with cTnT-miR-486 AAV9 within 30 min post myocardial reperfusion. Heart tissues were harvested at 3 weeks post cardiac ischemia/reperfusion (I/R) injury. (D) Western blot for AKT phosphorylation levels in

heart tissues from mice treated with cTnT-miR-486 AAV9 within 30 min post myocardial reperfusion. Heart tissues were harvested at 3 weeks post cardiac I/R injury (n=6). Data were compared by two-way ANOVA test followed by Tukey post hoc test. *, $P<0.05$; **, $P<0.01$; ***, $P<0.001$.

Figure S16. Expression of miR-486 in a mouse model of swimming exercise. (A) RT-PCR for the known factors in response to swimming exercise in heart tissues (n=6). (B) RT-PCR for circulating miR-486 levels in the serum from swimmed mice and sedentary mice (n=7-8). (C,D) RT-PCR for miR-486 expression in the gastrocnemius (C) and anterior tibialis (D) from swimmed mice and sedentary mice (n=3-6). Data were compared by unpaired two-tailed Student's t-test. *, $P<0.05$; **, $P<0.01$.

Figure S17. MiR-486 inhibition regulates fibrosis-associated gene markers and its downstream targets in swimmed mice upon cardiac ischemia/reperfusion injury. (A,B) RT-PCR for fibrosis-associated gene markers (A) and PTEN and FoxO1 (B) in mice heart tissues (n=6 for sedentary mice, n=11-12 for swimmed mice). Data were compared by two-way ANOVA test followed by Tukey post hoc test. ***, $P<0.001$.

Figure S18. The beneficial effect of swimming exercise against cardiac ischemia/reperfusion injury is attenuated in miR-486 knockout mice. (A) Schematic diagram showing that miR-486 knockout (KO) mice and wild type (WT) littermates were subjected to swimming exercise for 3 weeks before cardiac ischemia/reperfusion (I/R) injury for 24 hrs. (B) The 2,3,5-triphenyltetrazolium chloride (TTC) staining for the infarct size at 24 hrs after I/R injury as determined by the infarct size/area at risk (INF/AAR) ratio. The area at risk/left ventricle weight (AAR/LV) ratio represents the homogeneity of surgery (n=5). Data were compared by

unpaired two-tailed Student's t-test. **, $P<0.01$.

Supplemental Table

Table S1. List of primers used for the PCR analysis.

Gene	Primer sequence
rno_Pten forward	ATTGCCTGTGTGTGGTGA
rno_Pten reverse	TCCTCTGGTCCTGGTATGA
rno_FoxO1 forward	TGGGGCAACCTGTCGTA
rno_FoxO1 reverse	GGGCACACTCTTCACCATC
mmu_Pten forward	AGCCCTAACCCCAAGAAC
mmu_Pten reverse	ACAAGTCCCGATGAAACCT
mmu_FoxO1 forward	GTACAGCGCATAGCACCA
mmu_FoxO1 reverse	GCGACAGACAGAGTTCCC
hsa_Pten forward	CAGTCAGAGGCGCTATGTGT
hsa_Pten reverse	CACCTTTAGCTGGCAGACCA
hsa_FoxO1 forward	GGATGTGCATTCTATGGTGTACC
hsa_FoxO1 reverse	TTTCGGGATTGCTTATCTCAGAC
mmu_C/EBPβ forward	GGGGTTGTTGATGTTTTTGGT
mmu_C/EBPβ reverse	TCGAAACGGAAAAGGTTCTCA
mmu_CITED4 forward	CCTGGCATACGGCTCCTTC
mmu_CITED4 reverse	AGACTGCAGGTGCGTGCTAC
mmu_CPhar forward	CATGGATTTCTGGACCTCCTA
mmu_CPhar reverse	TTCATGGCTTTACAGCGT
rno_Smad1 forward	CGTGTTGGTGGATGGTTT
rno_Smad1 reverse	TGTGTCGCCTGGTATTTTC
rno_Smad2 forward	GTCAGTGCGATGCTCAAG
rno_Smad2 reverse	CTCAAGTGCTGTTTTCGCT
mmu_CTGF forward	TAAGACCTGTGGGATGGG
mmu_CTGF reverse	GCAGCCAGAAAGCTCAA
mmu_Col1a1 forward	TAAGGGTCCCCAATGGTGAGA
mmu_Col1a1 reverse	GGGTCCCTCGACTCCTACAT
mmu_Col3a1 forward	CTGTAACATGGAAACTGGGGAAA
mmu_Col3a1 reverse	CCATAGCTGAACTGAAAACCACC
mmu_BNP forward	GAGTCCTTCGGTCTCAAGGC
mmu_BNP reverse	TACAGCCCAAACGACTGACG